This is an *Accepted Manuscript*, which has been through the Royal Society of Chemistry peer review process and has been accepted for publication.

*Accepted Manuscripts* are published online shortly after acceptance, before technical editing, formatting and proof reading. Using this free service, authors can make their results available to the community, in citable form, before we publish the edited article. We will replace this *Accepted Manuscript* with the edited and formatted *Advance Article* as soon as it is available.

You can find more information about *Accepted Manuscripts* in the **Information for Authors**.

Please note that technical editing may introduce minor changes to the text and/or graphics, which may alter content. The journal's standard **Terms & Conditions** and the **Ethical guidelines** still apply. In no event shall the Royal Society of Chemistry be held responsible for any errors or omissions in this *Accepted Manuscript* or any consequences arising from the use of any information it contains.

# Four-Coordinate Nickel(II) and Copper(II) Complexes Based ONO Tridentate Schiff Base Ligands: Synthesis, Molecular Structure, Electrochemical, Linear and Nonlinear Properties, and Computational Study[†‡]

**Nestor Novoa,[a,b] Thierry Roisnel,[b] Paul Hamon,[b] Samia Kahlal,[b]**
**Carolina Manzur,[a] Hoang Minh Ngo,[c] Isabelle Ledoux-Rak,[c]**
**Jean-Yves Saillard,\*[b] David Carrillo\*[a] and Jean-René Hamon\*[b]**

[a]   *Laboratorio de Química Inorgánica, Instituto de Química, Pontificia Universidad Católica de Valparaíso, Avenida Universidad 330, Valparaíso, Chile. E-mail: david.carrillo@ucv.cl*

[b]   *UMR 6226 «Institut des Sciences Chimiques de Rennes», CNRS-Université de Rennes 1, Campus de Beaulieu, 35042 Rennes Cedex, France. E-mails: saillard@univ-rennes1.fr; jean-rene.hamon@univ-rennes1.fr*

[c]   *Laboratoire de Photonique Quantique et Moléculaire, UMR 8537 CNRS-ENS Cachan, Institut d'Alembert, 61 Avenue du Président Wilson, 94235 Cachan Cedex, France*

[†]   Dedicated to the memory of our esteemed colleague Dr. Guy Lavigne, in recognition of his contribution to ruthenium chemistry and homogeneous catalysis

1

**Abstract:**

We report the synthesis, characterization, crystal structures, nonlinear- optical (NLO) properties, and density functional theory (DFT) calculations of nickel(II) and copper(II) complexes based ONO tridentate Schiff base ligands: two mononuclear compounds, $[Ni(An-ONO)(NC_5H_5)]$ (**5**) and $[Cu(An-ONO)(4-NC_5H_4C(CH_3)_3)]$ (**6**), and two heterobimetallic species $[M(Fc-ONO)(NC_5H_5)]$ (M = Ni, **7**; Cu, **8**), where $An-ONOH_2$ (**3**) and $Fc-ONOH_2$ (**4**) are the 1:1 condensation products of 2-aminophenol and, respectively, p-anisoylacetone and ferrocenoylacetone These compounds were characterised by microanalysis, FT-IR and X-ray crystallography in the solid-state, and in solution by UV-vis and $^1H$ and $^{13}C$ NMR spectroscopy. The crystal structures of **3-5**, **7** and **8** have been determined and show for Schiff base complexes **5**, **7** and **8** a four-coordinated square-planar environment for the nickel and copper ions. The electrochemical behavior of all derivatives **3-8** was investigated by cyclic voltammetry in dichloromethane, and discussed on the basis of DFT-computed electronic structures of the neutral and oxidized forms of the compounds. The second-order NLO responses of **3-8** have been determined by harmonic light scattering measurements using a $10^{-2}$ M solution of dichloromethane and working with a 1.91 μm incident wavelength, giving rather high $\beta_{1.91}$ values of 350 and 290 x $10^{-30}$ esu found for the mononuclear species **5** and **6**, respectively. The assignment and the nature of the electronic transitions observed in the UV−vis spectra were analyzed using time-dependent (TD) DFT calculations. They are dominated by LMCT, MLCT and π-π* transitions.

## Introduction

In the recent years, new molecular architectures have been designed, synthesized and meticulously studied in order to satisfy requirements of the emerging optoelectronic and photonic technologies.[1,2] In this regard, organic and metal-organic compounds with second-order nonlinear optical (NLO) properties have been extensively investigated because of their potential applications in optoelectronic devices of telecommunications, information storage, optical switching, and signal processing.[3] The majority of studies focused on quadratic nonlinearities in one-dimensional dipolar push-pull molecules of [donor]-[electronic conjugated pathway]-[acceptor] type structure (D-$\pi$-A), which show several intense, low-energy electronic transitions and strong variations of the dipole moment during the electronic excitation.[4] Albeit organic compounds[5,6] have been the most widely investigated, organometallic and coordination complexes have gained considerable attention as second-order NLO chromophores because they display high environmental stability and offer the capability to vary the identity of the metal center and of its coordinated ligands, the oxidation state, and the coordination geometry, giving rise to tunable and usually high intensity and relatively low energy metal-to-ligand charge transfer (MLCT), ligand-to-metal charge transfer (LMCT), or intraligand charge transfer (ILCT) transitions.[7-10]

In this context, $N_2O_2$ Schiff base complexes have appeared to be a promising class of efficient chromophores exhibiting large NLO responses.[8b,h,11] The continuing interest[11a-13] for these salen-type Schiff base compounds[14] is mainly due to their preparative accessibility, ease of derivatization, and thermal stability. Interest for $N_2O_2$ Schiff base complexes comes also from the active role, strategic position, and nature (closed-shell vs. open-shell)[15] of the metal ion which is a constituent of the polarizable bridge in the D-$\pi$-A structure. In addition, they exhibits low energy charge-transfer transitions.[15] $N_2O_2$-based unsymmetrical tetradentate Schiff base ligands are easily prepared upon condensation of mono-condensed Schiff base precursors containing a terminal amino group with salicylaldehydes under mild conditions.[16,17] During the last decade, we successfully used this strategy to construct NLO active[18] neutral heterobimetallic and ionic heterotrimetallic organometallic donor-acceptor substituted unsymmetrical Ni(II)- and Cu(II)-centered $N_2O_2$ Schiff base complexes,[19] starting from ferrocenyl-functionalized enaminones.[20]

Remarkably, appropriate substitution of both tridentate enaminone half-unit[21] and salicylidene rings allows preparation of main-chain Schiff base oligomers possessing high second-order NLO responses.[22]

Studies on transition metal complexes containing a tridentate Schiff base ligand and an ancillary N-donor monodentate coligand occupying the fourth coordination site of the metal center have mainly been devoted to the determination of crystalline and molecular structures, factors affecting the nuclearity of complexes and magneto-structural correlations.[23,24] However, studies on their quadratic optical nonlinearities remained scarce,[13b,25] in spite of the exceptionally high second order NLO activity with $|\mu\beta|$ up to $3000 \times 10^{-48}$ esu (Electric-Field-Induced Second Harmonic Generation (EFISH) technique, incident wavelength 1.907 μm) reported by Sentore, Roviello and co-workers,[26] for mononuclear copper(II) and palladium(II) unsymmetrical complexes containing ONO donor N-salicylidene-N'-arylhydrazine tridentate ligands and pyridine. On the other hand, Density Functional Theory (DFT) calculations have been employed to investigate the second-order NLO properties of tridentate Schiff base complexes.[13c,27,28] The results show that these properties are sensitive to the exchange of donor/acceptor because of the differences of the extent of charge separation and the intraligand charge transfer (ILCT) processes.[28] Therefore, these systems still remain interesting for further investigations.

Here, as part of a program of investigating NLO active unsymmetrical Schiff base metal complexes, we centered our interest on the design of two new series of nickel(II)- and copper(II)-based unsymmetrical ONO tridentate Schiff base building blocks that could serve later on as molecular clips for the construction of self-assembled polynuclear push-pull systems, coordination polymers or supramolecular architectures. In this context, our main goal is to confirm that the first order (β) hyperpolarizabilities of these building blocks are strong enough to be used in the construction of nonlinear supramolecular objects, without requiring to reach the ultimate limits of β values.[29] For this aim, neutral ternary mononuclear and heterobimetallic complexes of the type [(R-ONO)M(II)(py)] (M = Ni, Cu; R = anisyl, ferrocenyl) and bearing a labile pyridine (py) ligand were prepared. Double deprotonation of the anisyl- and ferrocenyl-containing Schiff bases precursors **3** and **4**, respectively, leads to the formation of di-negative tridentate ONO donor ligands that react readily with metal(II) salts to produce their corresponding Ni(II) and Cu(II) complexes **5-8**

(see formulas in Scheme 1), in the presence of the nitrogenous co-ligand. The two Schiff base precursors and their four complexes have been thoroughly characterized by FT-IR, multinuclear NMR and elemental analysis. Their crystal structures have been determined by single crystal X-ray diffraction analysis. These new compounds have also been studied by UV-vis spectroscopy, cyclic voltammetry, DFT calculations and their nonlinear optical properties have been determined using the Harmonic Light Scattering (HLS) technique. In addition, DFT and its time-dependent DFT extension (TD-DFT) provide a rationalization of the electrochemical, spectroscopic and optical properties.

## Results and discussion

### Synthesis and characterization of the ligand precursors and complexes

The two diprotonated Schiff base ligands, $R-C(O)CH=C(CH_3)N(H)-o-C_6H_4OH$ (**3**: $R = 4-MeOC_6H_4$, **4**: R = Fc) , were prepared by facile monocondensation of 2-aminophenol with 1-anisyl-1,3-butanedione (**1**) and 1-ferrocenyl-1,3-butanedione (**2**), respectively, in refluxing toluene for 2 hours (Scheme 1). Compounds **3** and **4** were isolated in similar yields (88 and 86%) as colorless and orange microcrystals, respectively, upon recrystallization from diethyl ether. They are both air and thermally stable and soluble in common organic solvents except in petroleum ether (40-60 °C). On the other hand, the neutral mononuclear and heterobimetallic unsymmetrical ternary Schiff base complexes **5**, **7** and **8**, respectively, were synthesized following a simple one-pot three-step templated reaction. First, the diprotic enaminone compounds **3** and **4** were doubly deprotonated with a slight excess of $t-BuO^-K^+$ in THF at ambient temperature. Pyridine was then added to the dark red reaction mixture before dropwise addition of a THF solution of the appropriate hydrated metal(II) nitrate salt (Scheme 1). It is worth noting that the expected mononuclear copper(II) complex [(An-ONO)Cu(py)] bearing the anisyl substituted ONO tridentate ligand was never obtained whatever the amount of pyridine used. Instead, its doubly phenoxo bridged homobimetallic counterpart [(An-ONO)Cu]$_2$ was always formed.[23] The known compound **6** can, however, be prepared by using 4-*tert*-butylpyridine as N-donor ancillary ligand (Scheme 1).[23] Compounds **5-8** are isolated in reasonably good 72-75% yields as microcrystalline solids. They are thermally stable, air and moisture insensitive on

storage under ordinary conditions, exhibiting good solubility in common polar organic solvents but are not soluble in ethanol, diethyl ether and hydrocarbon solvents.
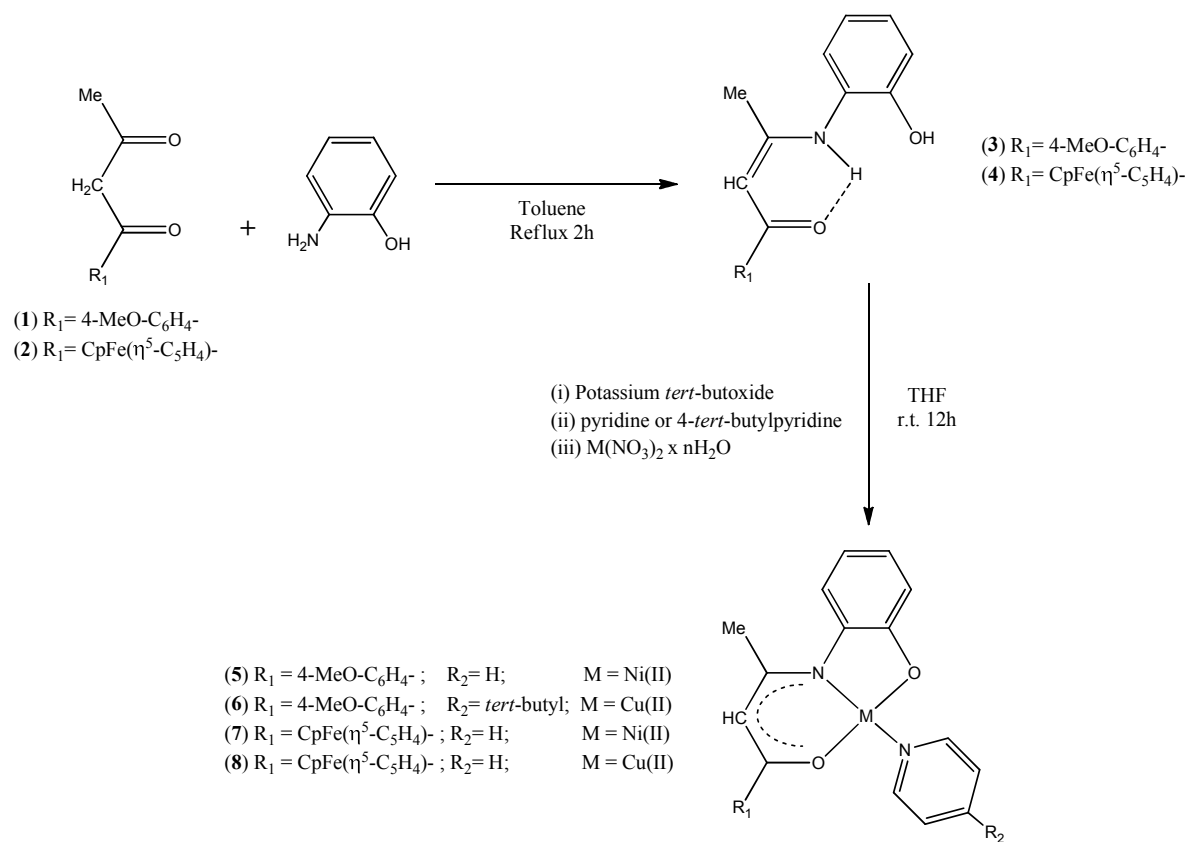


**Scheme 1** Synthesis of compounds **3-8**

Satisfactory elemental analysis, FT-IR, multinuclear 2D NMR and UV-vis spectroscopies, and single-crystal X-ray diffraction served to confirm the composition and identity of the five new compounds **3-5**, **7** and **8**. In addition, high resolution ESI-MS of the heterobimetallic derivatives **7** and **8** gave an exact mass of M/z= 496.03841 and 501,03267 for [M]$^+$ that matched the calculated values of 496.0385 and 501.0330, respectively, along with the expected isotopic distribution for the molecular ion peaks.

The solid-state FT-IR spectra of all the compounds **3-8** were assigned on the basis of frequency calculations on their DFT optimized geometries. Table S1 gathers both computed and experimental major frequencies and their respective attributions,[‡] showing a good agreement between the calculated and observed spectral data. In particular, the spectra

of the enaminonic compounds **3** and **4** exhibited (i) a strong and a broad medium stretching bands due to the O=C-C=C enone core at 1593/1532 and 1592/1537 cm$^{-1}$, respectively, and (ii) a weak symmetric and a strong deformation stretching modes of the *o*-phenylene O-H and enamine N-H groups, at 3150/1458 and 3073/1519 cm$^{-1}$ for **3**, and at 3427/1445 and 3377/1491 cm$^{-1}$ for **4**, respectively. Compared to free amines, the N-H vibrations appear at somewhat lower energy as a consequence of the N-H···O intramolecular hydrogen bond. As expected, those O-H and N-H absorption bands have vanished in the spectra of complexes **5-8**, indicating that the coordination to the metal ion has taken place through both deprotonated oxygen and nitrogen atom.

The formation of **3** and **4**, and of their corresponding diamagnetic complexes **5** and **7**, were readily noticed in their respective $^1$H NMR spectrum, showing in each case a pair of sharp singlets at $\delta_H$ 1.71/3.84 and 2.61/3.85 ppm assigned to the methyl and methoxy protons of **3** and **5**, respectively, and at $\delta_H$ 1.73/4.17 and 2.49/4.15 ppm attributed to the methyl and free cyclopentadienyl ring protons of **4** and **7**, respectively. One can immediately note that the methyl resonances are downfield shifted by 0.90 and 0.78 ppm upon coordination of the ligands to the Ni(II) metal ion and formation of the pseudo-aromatic six-membered metallacycles. Similarly, the vinylic C-H resonances observed at $\delta_H$ 5.67 and 5.30 ppm for **3** and **4**, respectively, moved downfield at $\delta_H$ 5.97 and 5.60 ppm in the spectra of **5** and **7**, respectively.

The two protonated ligands were obtained as their enaminone tautomeric forms, as deduced from their $^1$H NMR spectra recorded in CDCl$_3$ at 315 K for **3** and at 298 K for **4**, that showed deshielded amino proton signals at $\delta_H$ 12.27 and 11.80 ppm, respectively, due to hydrogen bonding between N-H and the C=O group. These downfield positions are in full agreement with the FT-IR data (see above) and also supported by the crystal structures (*vide infra*). The above mentioned solution behaviour, where no keto-imine tautomer can be detected, is similar to that reported for organic[30] and ferrocenyl-containing enaminones.[19b,21,31]

On the other hand, the asymmetry of the four compounds is clearly reflected by the four distinct resonances of the *o*-phenylene ring, in agreement with four magnetically non-equivalent protons (integral ratio 1:1:1:1). They appear mainly as doublets (H-3 and H-6) and triplets (H-4 and H-5) in the ranges $\delta_H$ 6.83 – 7.16 ppm for **3** and **4**, and $\delta_H$ 6.39-7.37

ppm for complexes **5** and **7**. Lastly, in both complexes **5** and **7**, the pyridine co-ligand gave rise to three resonances (integral ratio 2:1:2) with the *ortho* protons showing up as the most downfield shifted signals of the spectra at $\delta_H$ 8.73 and 8.62 ppm, respectively. One can also note that the spectrum of **7** has to be recorded at 253 K to get optimum resolution, suggesting some steric interaction between pyridine and the ferrocenyl moiety (Fig. S1). [‡]

The proton decoupled $^{13}$C NMR spectra confirmed the unsymmetrical nature of the four compounds with the expected number of resonances, except for **7** where the carbon nuclei of the pyridine co-ligand were not observed (see Experimental for complete assignments). For instance, spectra of **3** and **4** confirm the existence of the keto-enamine tautomeric form for both species with the methyne carbon (C-9) resonating at $\delta_C$ 94.30 and 95.80 ppm, respectively. Those signals are downfield shifted by 6.70 and 5.46 ppm upon complexation to form **5** and **7**, respectively, while in both cases the carbonyl carbon (C-10) experienced a upfield shift of about 20 ppm upon coordination of the oxygen atom to the nickel center.

### X-ray Crystal Structures

Diffraction-quality single crystals for X-ray structure investigation were obtained for compounds **3**, **4**, **5**, **7** and **8** by slow evaporation of the solvent from a saturated solution of the compound in either dicloromethane or diethyl ether (see Experimental). The molecular structures are shown in Fig. 1-3, and selected bond lengths and angles are listed in Tables S2-S4.[‡] The single-crystal X-ray diffraction studies confirm that each compound contains the ONO Schiff base framework resulting from the monocondensation of the appropriate β-diketones and 2-aminophenol, bearing the anisyl group in **3** and **5** and the ferrocenyl moiety in **4**, **7** and **8**. In those latter three compounds, the ferrocenyl unit features a typical linear $\eta^5$-Fe-$\eta^5$ sandwich structure.[32] The cyclopentadienyl rings are parallel and, depending on the compound, are either totally eclipsed or staggered. The measured ring centroid-iron distances, averaging 1.655 and 1.652 Å for the free and substituted ring, respectively, are in agreement with a Fe(II) oxidation state in the metallocenyl units (Table S5).[‡] The other aspects of the structures are discussed below in three sections for the sake of simplicity.

*Ligand precursors 3 and 4.* The organic enaminone **3** crystallizes in the tetragonal noncentrosymmetric space groups P-421c, while its organometallic counterpart **4** crystallizes in the triclinic centrosymmetric space groups P͞1 with three crystallographically nonequivalent molecules (**4A-C**) found in the unit cell. The molecular structures (Fig. 1) show that both compounds exist as the *Z-s-Z* conformational form,[33] consistent with a keto-enamine tautomeric isomer for **3** and **4** with an intramolecular O(2)··H-N(1) hydrogen bond (Table S6)[‡] that closes the planar pseudo six-membered [O(2)-C(10)-C(9)-C(7)-N(1)] ring through the resonant ··O=C-C=C-NH·· fragment,[34] with alternating double-, single-, double- and single-bonds[35] between the vicinal $sp^2$-hybridized atoms (Table S2).[‡] The metrical parameters of **3** and **4** are in accordance with previously reported structural data for enaminone derivatives.[19b,21,31,36] In addition, the structure of the organometallic enaminone **4** is stabilized by intermolecular hydrogen bonds formed between the hydrogen atom of the hydroxyl group and the oxygen atom of a carbonyl unit of a neighboring molecule (Table S6 and Fig. S2).[‡]
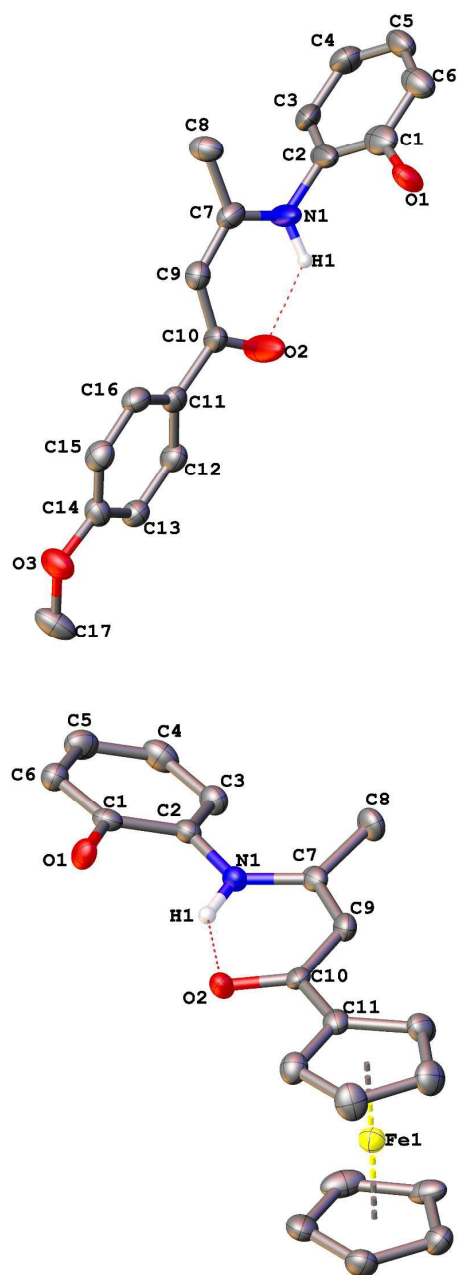
**Fig. 1** Molecular structures of **3** (top) and **4** (molecule **A**, bottom) with atom numbering schemes. Hydrogen atoms have been omitted for clarity. Thermal ellipsoids are drawn at 60% probability.

*Mononuclear complex 5.* The mononuclear nickel(II) complex **5** crystallizes in the orthorhombic noncentrosymmetric space groups $P2_1\,2_1\,2_1$ with two crystallographically nonequivalent molecules (**5A,5B**) found in the asymmetric unit. The compound consist of a tetracoordinated Ni(II) metal ions in a square-planar environment, with the coordination sphere formed by the deprotonated amide nitrogen atom and the carbonyl and phenolato oxygen atoms of the chelating Schiff base ligand, and of the nitrogen atom of the pyridine co-ligand (Fig. 2), forming monomeric entities that are separated by normal van der Waals distances. By contrast, its copper(II) counterpart **6** packs as dimers. The metal center is pentacoordinated, exhibiting a square pyramidal coordination geometry.[23] However, the basal plane is made of the same ONO donor set of atoms and of the nitrogen atom of the 4-*tert*-butylpyridine. The apical site is occupied by the phenoxido oxygen atom of the ONO tridentate ligand that is basal to the second cupric metal ion of the dimeric unit.
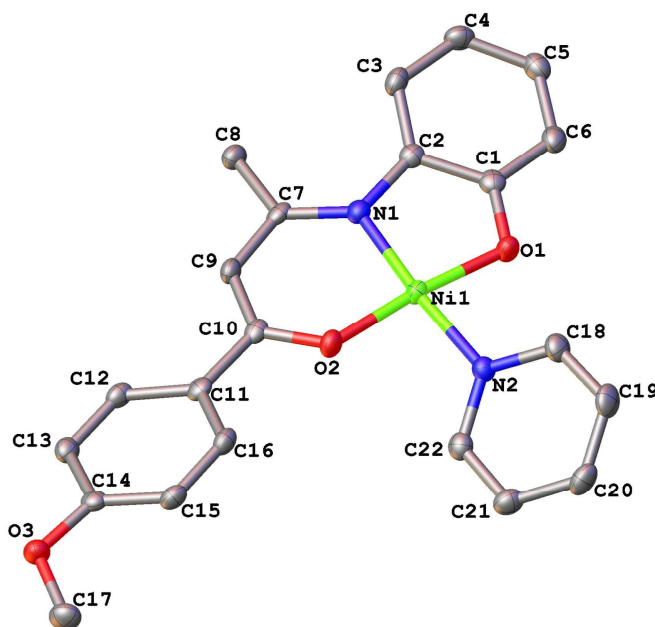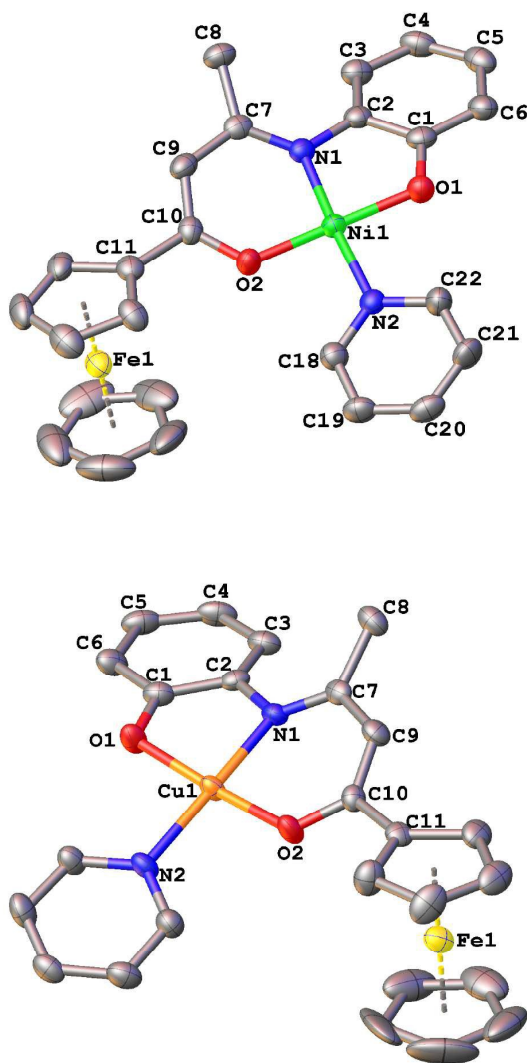


**Fig. 2** Molecular structure of **5** (molecule **A**) with atom numbering schemes. Hydrogen atoms have been omitted for clarity. Thermal ellipsoids are drawn at 60% probability.

In the square planar arrangement around the Ni(II) center, the four donor atoms adopt a $N_2O_2$ *trans*-configuration. The sum of the bond angles involving the metal and the donor set of atoms are of 360.04 and 360.10° in **5A** and **5B**, respectively, and the O(1)-Ni-O(2) and N(1)-Ni-N(2) diagonal angles are about 175° (Table S3).[‡] In **6**, the O(1)-Cu-O(2) transoid angle is of the same order but the N(1)-Cu-N(2) angle is of 162.66(5)°, strongly deviating from linearity. The bond distances of the donor atoms of the tridentate Schiff base ligand to the central metal ion span the range 1.8229(14) – 1.8801(18) Å (Table S3),[‡] and are typical of ternary square-planar Ni(II) complexes.[24e] The NI(1)-N(2) bond distances of 1.9315(17) in **5A** and 1.9380(17) in **5B**, are slightly longer as expected for a weaker coordinating neutral ligand. However, they remain shorter by 0.04 Å tan the Cu(1)-N(2) distance of 2.0467(13) Å measured in compound **6**, taking into account the ionic radius of each metal ion.[37]

The fused five- and six-membered heterometallacycles formed upon chelation of the Ni(II) metal ion are essentially co-planar, making dihedral angles of 17.5(1) and 26.7(1)° with the anisyl substituent, in **5A** and **5B**, respectively, whereas the pyridine co-ligand is twisted by 30.8(1) and 37.9(1)° with respect to the coordination plane. In compound **6**, the anisyl group is co-planar with the coordination plane while the 4-*tert*-butylpyridine makes a dihedral angle of 25.60(3)°.[23] In addition, The bond lengths and angles of the Schiff base skeleton (Table S3),[‡] are indicative of substantial $\pi$ delocalization of the electron density through the entire heterometallacycles framework.

***Heterobimetallic complexes 7 and 8.*** The heterobimetallic nickel Schiff base complex **7** crystallizes in the orthorhombic centrosymmetric space group P*cab*, while its copper counterpart **8** crystallizes in the monoclinic centrosymmetric space groups P2$_1$/*a*, with two crystallographically nonequivalent molecules (**8A,8B**) found in the asymmetric unit. The two structures are almost identical, differing only by the nature of the centered metal ion that is four-coordinated by a ferrocenyl-containing ONO tridentate Schiff base ligand and a pyridine as ancillary ligand (Fig. 3), forming monomeric units that are separated by normal van der Waals distances. In both **7** and **8**, the centered M(II) ion adopt a square planar geometry with the nitrogen and oxygen atoms occupying mutually *cis*

12

positions. This is reflected in the O(1)-M-O(2) and N(1)-M-N(2) diagonal angles ranging between 174.52(10) and 177.08(10)° (Table S4),‡ barely deviating from linearity.



**Fig. 3** Molecular structures of **7** (top) and **8** (molecule **A**, bottom) with atom numbering schemes. Hydrogen atoms have been omitted for clarity. Thermal ellipsoids are drawn at 60% probability.

The bond lengths and angles around the centered metal ions (Table S4)[‡] are very similar to those measured in their respective mononuclear counterparts **5** and **6** (see Table S3).[‡] As expected, the M-N(2) bond distances remain the larger ones, increasing on passing from **5** (1.9315(17), 1.9380(17) Å) to **7** (1.964(3) Å), but decreasing on passing from **6** (2.0467(13) Å) to **8** (2.023(2), 2.028(2) Å). In both complexes, the fused five- and six-membered heterometallacycles are essentially co-planar and form with the substituted cyclopentadienyl ring of the ferrocenyl moiety, dihedral angles of 22.0(1)°, 18.7(2) and 17.9(2)° for **7**, **8A** and **8B**, respectively, while the pyridine plane is twisted by 16.4(1)°, 15.1(1) and 14.6(1)° with respect to the coordination core. Additionally, interatomic distances, found between single and double bond lengths,[34] and angles close to 120° of the chelating Schiff base ligand (Table S4),[‡] suggest as in compound **5** above, substantial $\pi$ delocalization of the electron density through the chelate rings. Moreover, a close inspection of the N(1)-C(7), C(7)-C(9), C(9)-C(10) and C(10)-O(2) bond distances (Table S7)[‡] suggests that the N-C=C-C=O system of the complex has more delocalization than that of the corresponding ligand precursor.

### Electronic absorption spectra

The electronic absorption spectra in the UV-visible region for the ligand precursors **3** and **4**, as well as their corresponding complexes **5-8**, were measured in $CH_2Cl_2$ and in DMSO solutions (Fig. S3).[‡] The spectra are mainly composed of two broad absorption bands whose nature of the involved transitions and their principal components have been assigned based on TD-DFT calculations (see below, Theoretical investigations). In addition, on moving from $CH_2Cl_2$ ($\varepsilon = 8.90$) to the more polar DMSO solvent ($\varepsilon = 47.6$), the low-energy absorption bands exhibit significant red shifts, except compound **3** that presents a hypsochromic shift and complex **7** for which the spectra remain unchanged (Table 1). Such a behavior is indicative of a positive change in the dipole moment between the excited and the ground states. It is also characteristic of push-pull complexes, and responsible for the NLO properties of these molecules. As the higher energy absorption band does not exhibit this solvent shift, we can assume that the corresponding excited state does no significantly contribute to the $\beta$ value according to the 2-level dispersion model.[38]

**Table 1** Experimental optical absorption maxima of the low-energy band for compounds **3-8**

| Compd | λ/nm (log ε) (CH₂Cl₂) | λ/nm (log ε) (DMSO) | Solv. Shift (cm⁻¹) |
|---|---|---|---|
| **3** | 365(4.59) | 343(4.52) | *-1757* |
| **4** | 339(4.38) 473(3.34) | 369(3.61) - | *+2398* - |
| **5** | 407(3.90) | 418(4.15) | *+646* |
| **6** | 408(4.24) | 431(3.93) | *+1308* |
| **7** | 413(3.92) | 413(3.53) | 0 |
| *8* | 411(4.34) | 426(4.12) | *+857* |

### Quadratic Nonlinear Optical Studies

The quadratic nonlinear responses of the Schiff base derivatives **3**-**8** have been determined at 1.91 µm incident wavelength using the HLS technique (see Experimental for details). The HLS measurements were carried out in dichloromethane solutions for all the compounds. The experimental $\beta_{1.91}$ values of the multipolar first hyperpolarizability, along with the dispersion-free intrinsic first hyperpolarizability ($\beta_0$) of these compounds, that have been calculated using the two-state model,[38] $\beta_0 = \beta_{1.91}(1-(\lambda_{max}/\lambda)^2)(1-(2\lambda_{max}/\lambda)^2)$, where $\lambda_{max}$ is the experimental optical absorption maximum and $\lambda$ is the fundamental wavelength of the laser, are presented in Table 2. This dispersion correction using the two-state model, previously applied to Schiff base linked aromatic and ferrocenyl complexes,[39] can be employed since compounds **3**-**8** have the MLCT band far away from the second harmonic

frequency,[40] and because one of the two absorption band, being insensitive to solvent effects, cannot significantly contribute to the β values as explained above.

**Table 2** HLS $\beta$ values determined at $\lambda_{inc}$ 1.91 μm for the Schiff base derivatives **3-8**[a]

| Compd | $\lambda_{max}$ (nm)[b] | $\beta_{1.91}$ ($10^{-30}$ esu)[c] | $\beta_0$ ($10^{-30}$ esu)[d] |
|-------|------|------|------|
| **3** | 365 | 150 | 120 |
| **4** | 339 | 130 | 110 |
| **5** | 407 | 350 | 270 |
| **6** | 408 | 290 | 220 |
| **7** | 413 | 170 | 130 |
| **8** | 411 | 170 | 130 |

[a]Relative experimental error on $\beta$ value is ± 10%. [b]Optical absorption maximum. [c]$10^{-2}$ M solution in $CH_2Cl_2$. [d]Values extrapolated to zero frequency.

Within the 10% measurement uncertainty, the $\beta_{1.91}$ values determined for compounds **3** and **4** are similar, thus confirming the similar electron donating capabilities of the anisyl and of the ferrocenyl groups.[5d] Within these bounds, the identical $\beta_{1.91}$ and $\beta_0$ values obtained for the heterobimetallic species **7** and **8** (Table 2) are also similar to that found for their common starting enaminone **4**. This is surprising as complexation of **3** and **4** by Ni(II) and Cu(II) ions is accompanied by the formation of a geometrically constrained planar structure which is expected to enhance the conjugation and, hence, the nonlinear efficiency. The observed NLO responses for **7** and **8**, twice smaller than those determined for their respective anisyl counterparts **5** and **6** (Table 2), could arise from steric hindrance, in accordance with NMR observations (see above), generating a substantial <u>twist</u> of the ferrocenyl moieties that may be a barrier to efficient intramolecular charge transfer. [41]

On the other hand, the coordination of the doubly deprotonated form of ligand precursor **3** to the [M(py)] fragment caused a dramatic difference in the second-order NLO responses. The hyperpolarizability values of 350 and 290 x $10^{-30}$ esu found for **5** and **6**, respectively, can be explained by a good participation of the anisyl substituent in the extended π-conjugated system. The barely weaker NLO response observed for complex **6** could result from a weaker push-pull effect due to the replacement of the pyridine by a more electron-rich *tert*-butylpyridine, in conjunction with a longer M-N bond distance (see Table S3). Those $\beta_{1.91}$ values are rather large for small conjugated macroacyclic molecules such as **5** and **6**,[7a,b,8b] and are higher than those we determined previously under the same experimental conditions for more extended unsymmetrical Schiff base chromophores.[18,22] Moreover, the nature of the electronic distribution of the square-planar metal ions ($d^8$ Ni(II) closed-shell *vs.* $d^9$ Cu(II) open-shell), either in **5/6** or **7/8** couples, does not play any role on the NLO properties.[8b,42] In addition, [(An-ONO)Ni(py)] (**5**) crystallizes in the noncentrosymmetric P2$_1$ 2$_1$ 2$_1$ space group which leads to a nonvanishing NLO response in the solid state. The ccompound therefore exhibits an second harmonic generation efficiency roughly equal to 0.9 times that of potassium dihydrogen phosphate, [43] determined by the Kurtz-Perry powder test.[44]

### Theoretical investigations

In order to get a better insight into the bonding and properties of compounds **3-8**, we have carried out DFT and TD-DFT calculations on these compounds, except for **6** which was slightly simplified in **6'** (see Computational details). Details of the calculations are given in the Experimental section. Their fully optimized geometries (in vacuum) are shown in Fig. S4[‡] and corresponding relevant metrical data are provided in Tables S2-S4.[‡] There is a good overall agreement between the X-ray and optimized structures, the experimental metal-ligand bond distances being slightly overestimated by DFT, as expected for complexes of electron-rich metals. The MO diagrams of **3** and **5** are shown in Fig. 4, those of their ferrocenyl relatives **4** and **7** on Fig. 5, whereas those of the copper complexes **6'** and **8** are provided in Fig. S5 and S6.[‡] For the sake of consistency with the TD-DFT calculations (see below), they correspond to single-point B3LYP calculations on the optimized PW91 geometries (both calculations including solvent effect). Still, the level

17

ordering and MO natures are quite insensitive of the chosen functional or solvent effect (only inversion of nearly degenerate levels can be noticed upon such changes). The HOMO of **3** is of π-type and mainly localized on the central C10/C9/C7/N1 unit with some phenolate admixture. On the other hand, the π-type HOMO-1 is mainly localized on the $R_1$ and phenolate ends of the molecule. The LUMO is π-bonding on the C11/C10/C9 backbone and antibonding with the neighboring atoms. The MO diagram of **5** is somewhat different from that of **3** for two reasons. One is that **3** is now deprotonated and therefore its electronic structure is somewhat modified and the other reason is its complexation by a Ni(pyridine) moiety. This complexation comes along with the appearance of four occupied non-bonding 3d(Ni) levels, of which only two (the HOMO-2 and HOMO-4) appear in the energy window of Fig. 4. The HOMO and HOMO-1 can be related to the HOMO-1 and HOMO-2 of **3**. Whereas the LUMO of **5** is similar to that of **3**, just above appear three new (and expected) levels, namely the two π*-pyridine orbitals encompassing the metal-ligand antibonding $d_{x2-y2}$ orbital.

The presence of a ferrocenyl substituent in **4** and **7** induces the existence of three high-lying occupied non-bonding 3d(Fe) orbitals (the "$t_{2g}$" set). In the case of **4**, they constitute three among the four highest occupied MOs (Fig. 5). Only the HOMO-2 has a large organic nature and resembles the HOMO of **3**, with some iron admixture. The LUMO of **4** is similar to that of **3**. The highest occupied levels of **7** are similar to those of **4**, but with the "organic" HOMO related to the HOMO-2 of **4**. Unsurprisingly, the lowest vacant orbitals of **7** are similar to those of **5**.

The MO diagrams of the copper(II) complexes **6'** and **8** (Figs. S5 and S6)‡ are strongly related to those of their nickel(II) relatives **5** and **7**, but with one supplementary electron occupying the metal-ligand antibonding $d_{x2-y2}$ SOMO, the later having more ligand than metal character. The spin density plots of these two complexes are shown in Fig. 6. Consistently with the significant ligand character of their SOMO, the computed Cu spin density of **6'** and **8** is 0.43 and 0.45, respectively. The other frontier orbitals of **6'** and **8** are the same as those of **5** and **7**.
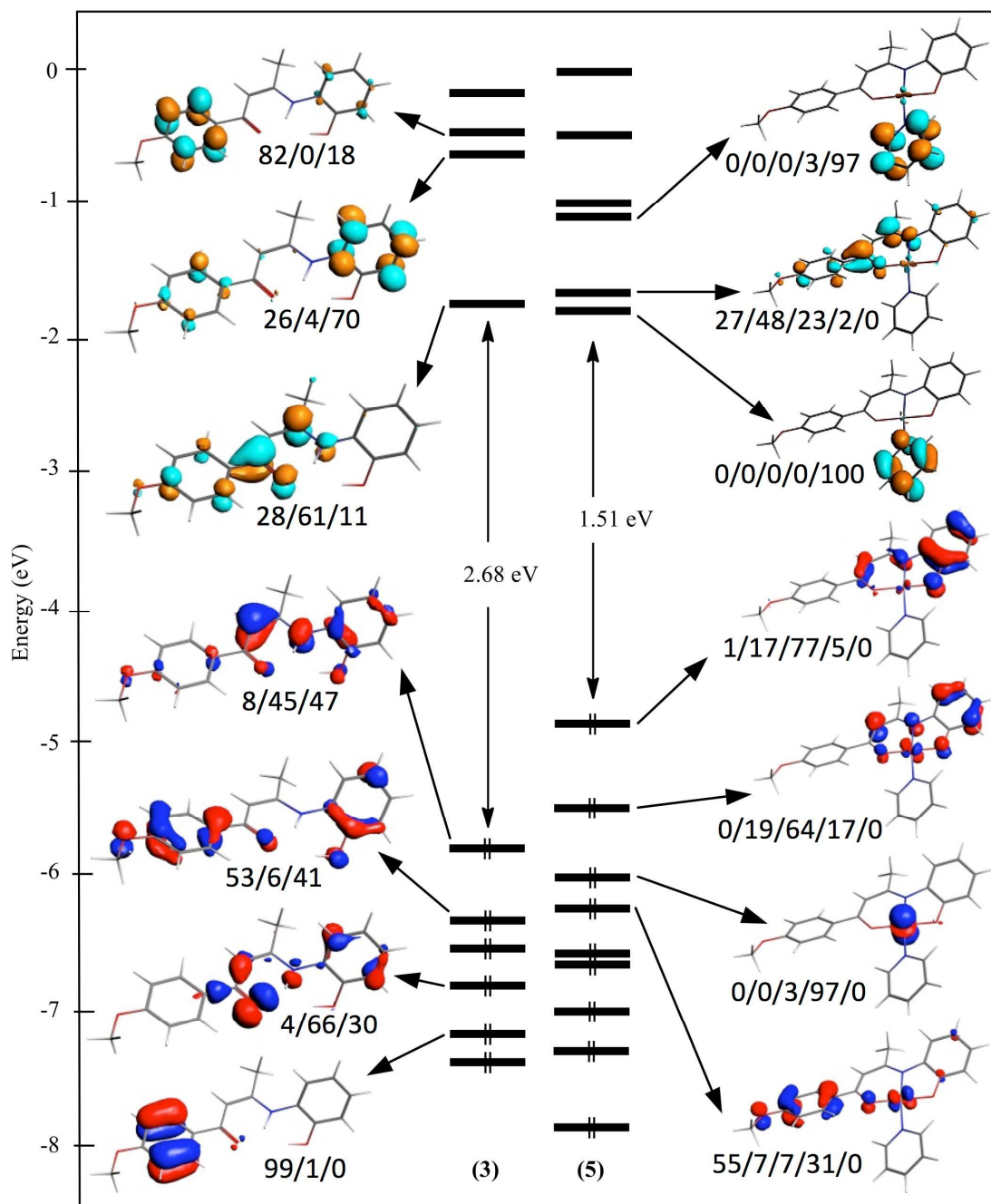
**Fig. 4** MO diagram of **3** and **5**. The MO localizations (in %) are given in the following order: $R_1$/C(10)[O(2)]-C(9)-C(7)[C(8)]-/-N(1)-$C_6H_4$-O(1) for **3** and $R_1$/C(10)[O(2)]-C(9)-C(7)[C(8)]-/-N(1)-$C_6H_4$-O(1)/M(II)/pyridine for **5**.
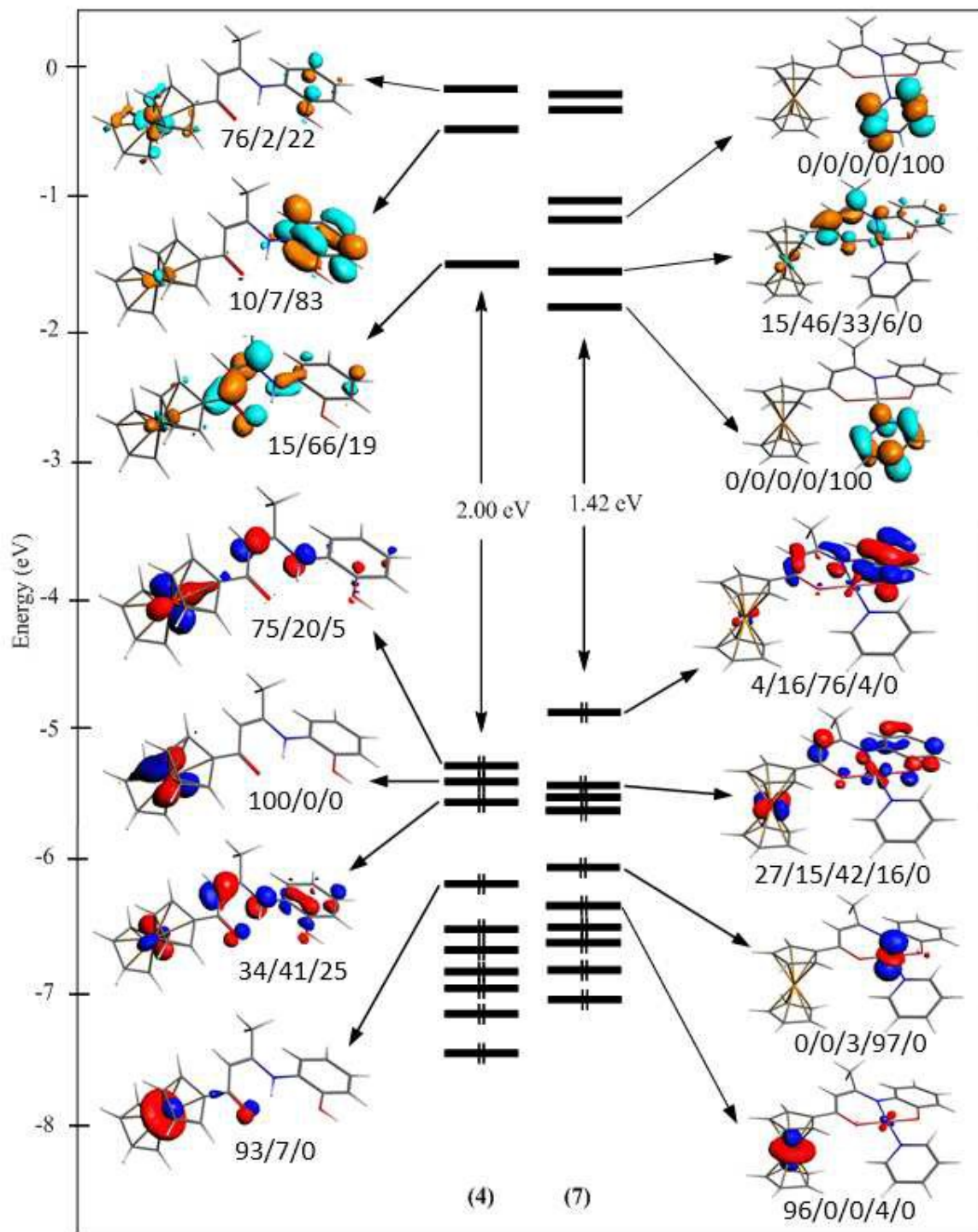
**Fig. 5** MO diagram of **4** and **7**. The MO localizations (in %) are given in the following order: R₁/C(10)[O(2)]-C(9)-C(7)[C(8)]-/-N(1)-C₆H₄-O(1) for **4** and R₁/C(10)[O(2)]-C(9)-C(7)[C(8)]-/-N(1)-C₆H₄-O(1)/M(II)/pyridine for **7**.

**6'**                                    **8**
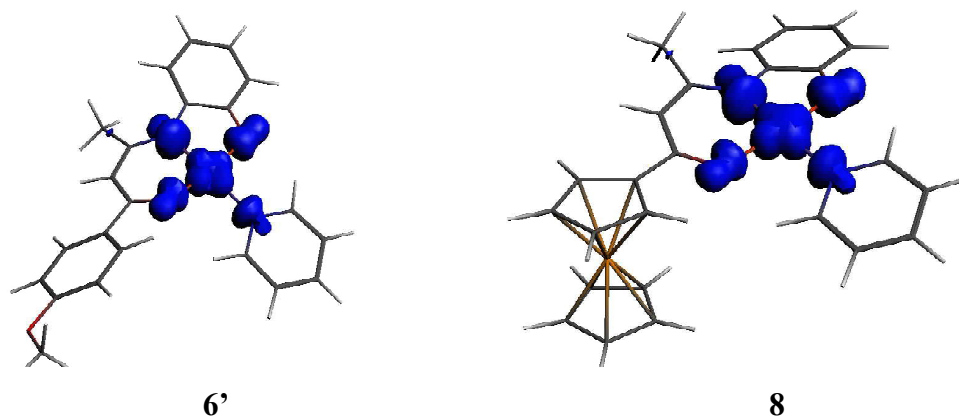
**Fig. 6** Spin density plot of complex **6'** and complex **8**

       The lowest UV-vis absorption transitions of **3-5**, **6'**, **7** and **8** have been computed by the means of TD-DFT calculations (see Computational details). The corresponding simulated spectra (solvent effect considered) are plotted together with the experimental ones of **3-8** in Fig. 7-9. The main features of the experimental spectra are satisfactorily well reproduced by the calculated spectra. This allowed us to propose band indexations from the analysis of the main components of the different computed transitions. These band indexations are summarized in Table 3. No strong trend can be traced from this table, except that the first transitions (bands **b**, **c**, **d**) are dominated by $\pi \rightarrow \pi^*$, and to a lesser extent, MLCT transitions. Interestingly, in the case of the pyridine complexes this ligand is never involved in these transitions, despite of the presence of vacant low-lying MOs of $\pi^*$-pyridine character. This is due to the lack of delocalization of these orbitals on the other parts of the molecules.

**Table 3** UV-vis $l_{max}$ experimental values and corresponding major computed optical transitions[a] with their dominant contributions (all wavelengths in nm).

| Compound | $l_{max}$(exp.)[b] | $l_{calc.}$ (major transitions)[c] | Principal components to the transitions | Nature of the transition |
|---|---|---|---|---|
| **3** | 280 (band **a**) | 316 (0.191) | HOMO-1 → LUMO | $\pi\rightarrow\pi^*$ |
| | 365 (band **b**) | 367 (0.968) | HOMO → LUMO | $\pi\rightarrow\pi^*$ |
| **4** | 277 (band **a**) | 273 (0.111) | HOMO → LUMO+1 | $\pi\rightarrow\pi^*$ + M(Fe)LCT (minor) |
| | 339 (band **b**) | 374 (0.744) | HOMO-2 → LUMO | $\pi\rightarrow\pi^*$ + M(Fe)LCT |
| | 464 (band **c**) | 532 (0.023) | HOMO → LUMO | M(Fe)LCT |
| **5** | 289 (band **a**) | 303 (0.108) | HOMO-4 → LUMO | M(Ni)LCT |
| | 416 (band **b**) | 380 (0.090) | HOMO → LUMO+2 | LM(Ni)CT + $\pi\rightarrow\pi^*$ (minor) |
| | 449 (band **c**) | 436 (0.829) | HOMO → LUMO | $\pi\rightarrow\pi^*$ |
| **6/6'** | 280 (band **a**) | 300 (0.305) | HOMO-5β → LUMOβ | LM(Cu)CT + $\pi\rightarrow\pi^*$ (minor) |
| | 344 (band **b**) | 342 (0.192) | HOMO-1β → LUMO+1β | $\pi\rightarrow\pi^*$ + M(Cu)LCT (minor) |
| | 404 (band **c**) | 437 (0.444) | HOMO-1α → LUMOα | $\pi\rightarrow\pi^*$ + LM(Cu)CT (minor) |
| **7** | 280 (band **a**) | 366 (0.156) | HOMO-3 → LUMO | $\pi\rightarrow\pi^*$ + M(Fe+Ni)LCT (minor) |
| | 413 (band **b**) | 420 (0.579) | HOMO → LUMO | $\pi\rightarrow\pi^*$ + M(Fe)LCT (minor) |
| | 456 (band **c**) | 534 (0.025) | HOMO-1 → LUMO | M(Fe)LCT |
| **8** | 279 (band **a**) | 302 (0.124) | HOMOβ-5 → LUMOβ | M(Fe) →M(Cu) |
| | 338 (band **b**) | 341 (0.05) | HOMO-2β → LUMOβ+2 | M(Fe)LCT |
| | 400 (band **c**) | 413 (0.420) | HOMOβ → LUMOβ+1 | n→π* + M(Fe)LCT (minor) |
| | 462 (band **d**) | 540 (0.03) | HOMOα → LUMOα | $\pi\rightarrow\pi^*$ + M(Fe)LCT (minor) |

[a] B3LYP calculations including solvent ($CH_2Cl_2$) corrections (see computational details). [b] Values recorded in $CH_2Cl_2$. [c] computed oscillator strength in parenthesis.

22
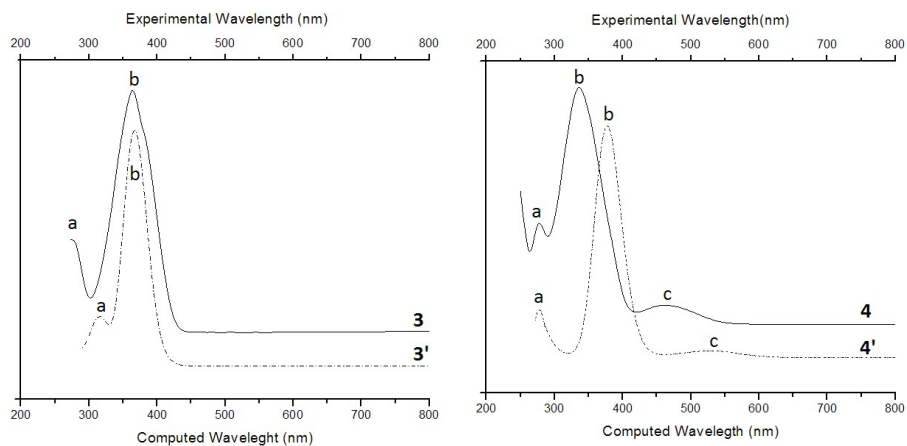
**Fig. 7** Experimental electronic spectra (top, full line) registered at 298 K in $CH_2Cl_2$ and simulated electronic spectra (bottom, dashed line) of **3** and **4**.
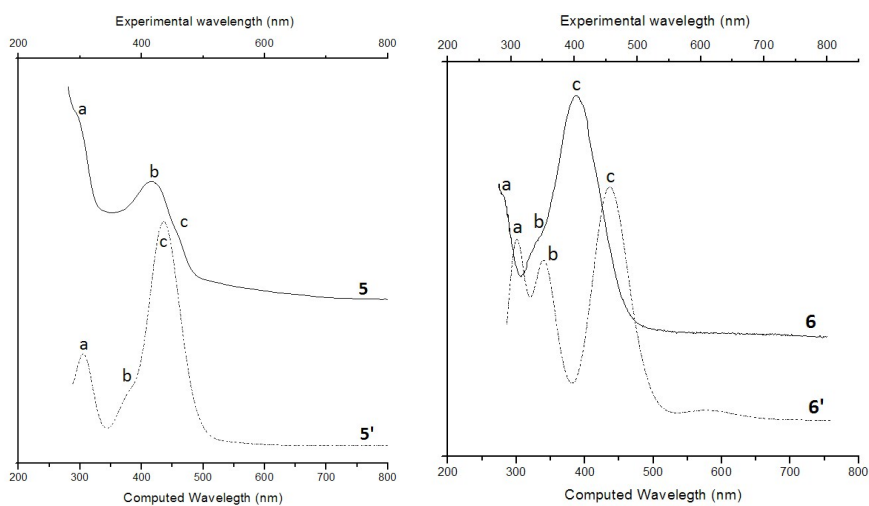


**Fig. 8** Experimental electronic spectra (top, full line) registered at 298 K in $CH_2Cl_2$ and simulated electronic spectra (bottom, dashed line) of **5** and **6'**.

23
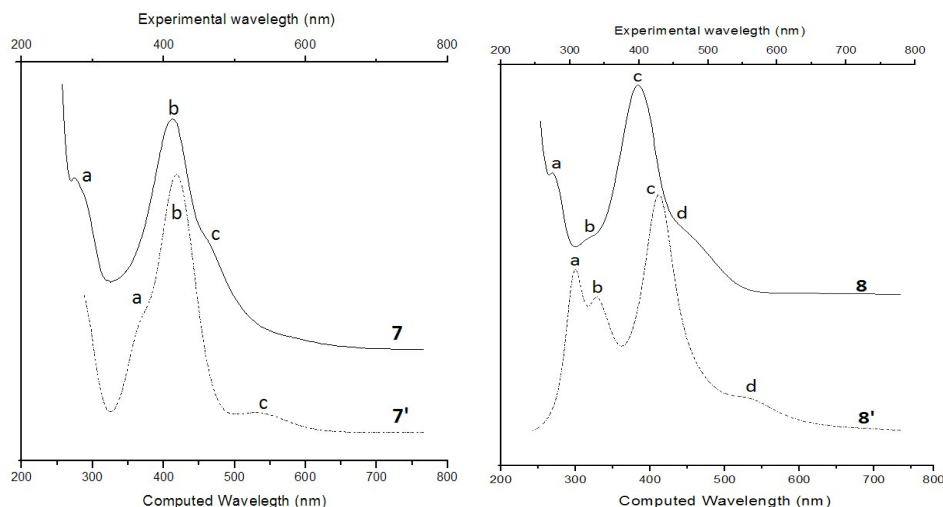
**Fig. 9** Experimental electronic spectra (top, full line) registered at 298 K in CH$_2$Cl$_2$ and computed electronic spectra (bottom, dashed line) calculated using B3LYP hybrid functional with COSMO/CH$_2$Cl$_2$ solvent effect of **7** and **8**.

### Electrochemical study

The redox behavior of compounds **3-8** has been investigated by cyclic voltammetry (CV) in dichloromethane solutions, at room temperature, in the potential range -1.00 to 2.00 V versus Ag/AgCl reference electrode. An interpretation of this behavior is proposed from the DFT-computed electronic structures of the neutral and oxidized forms of these compounds. The cyclovoltammogram of the protonated ligand **3** exhibits an irreversible oxidation wave at $E_{pa}$ = 1.37 V, which can be tentatively attributed to the [$o$-HO-Ph]/[$o$-HO-Ph]$^+$ couple.[45] As exemplified by the computed spin density plot of **3**$^+$ (Fig. S7),[‡] this oxidation corresponds mainly to the depopulation of the HOMO of **3** (see Fig. 4) which has a significant $o$-HO-Ph character but is fairly delocalized on the π-type backbone. The CV of the organometallic precursor **4** (Fig. 10) shows a quasi-reversible oxidation process, due to the monoelectronic oxidation of the ferrocenyl moiety,[46,47] with current ratio $i_{pa}/i_{pc}$ equal to 0.95, at $E_{1/2}$ = 0.90 V, with anodic to cathodic peak-to-peak separation ($\Delta E_p$) of 100 mv. The anodically shifted $E_{1/2}$ value is in accordance with previously measured redox potentials for ferrocenoyl-containing compounds.[48] The spin density plot of **4**$^+$ (Fig. S7),[‡] is consistent with the depopulation of the HOMO of **4** (see Fig. 5), the computed Fe spin density of **4**$^+$ being 0.75. Besides the reversible Fe(II)/Fe(III) redox process, the CV of **4**

displays also the irreversible oxidation waves of the phenol entity at $E_{pa}$ = 1.54 V (Fig. 10). This more positive response relative to that found for **3**, is expected as the consequence of the electrogenerated cationic ferrocenium substituent onto the molecule. The **$4^{2+}$** spin density plot of its triplet ground state (Fig. S7)[‡] confirms this attribution as well as an important participation of iron to this second oxidation (the Fe spin density increases to +1.21).

The CV of complex **5** shows two irreversible oxidation processes. The first redox event appearing at $E_{pa}$ = 0.87 V *vs.* Ag/AgCl, can be attributed to the Ni(II)-phenolato/Ni(II)-phenoxyl redox system,[49] as exemplified by the spin density plot of **$5^+$** (Fig. S7)[‡] which indicates depopulation of the HOMO of **5**, with minor metal participation. The second oxidation wave at $E_{pa}$ = 1.20 could be tentatively referred to the Ni(II)/Ni(III) couple.[49] However, our DFT calculations on **$5^{2+}$** indicate a singlet ground state, consistent with full depopulation of the HOMO of **5**. It is noteworthy that a similar result has been found for a related Ni(II) system.[50] The CV of complex **6** is similar to that of **5** and shows also two irreversible oxidation processes.[51] The first one at $E_{pa}$ = 0.72 v *vs.* Ag/AgCl is associated with the depopulation of the metal($d_{x2-y2}$)-ligand antibonding SOMO which becomes the LUMO of the strongly preferred singlet ground state of **$6^+$**, after admixing significant π-type phenolato character. Interestingly, our DFT results on **$6'^{2+}$** indicate that the second oxidation wave recorded at 1.04 V *vs.* Ag/AgCl can be approximated to the relocalization of the unpaired electron on the metal($d_{x2-y2}$)-ligand antibonding MO, however with some ligand π-type participation (metal spin density = 0.39; see also Fig. S7),[‡] associated with full depopulation of a phenolato π-type bonding MO, similarly to **$5^{2+}$**.

The cyclic voltammograms (Fig. 10) of the heterobimetallic derivatives **7** and **8** are similar and display both two quasi-reversible one-electron oxidation waves at $E_{1/2}^1$(**7**) = 0.65 V ($i_{pa}/i_{pc}$ equal to 0.93, $\Delta E_p$ = 70 mV), $E_{1/2}^2$(**7**) = 0.93 V ($i_{pa}/i_{pc}$ equal to 0.90, $\Delta E_p$ = 160 mV), and $E_{1/2}^1$(**8**) = 0.63 V ($i_{pa}/i_{pc}$ equal to 0.92, $\Delta E_p$ = 60 mV)and $E_{1/2}^2$(**8**) = 0.94 V ($i_{pa}/i_{pc}$ equal to 0.97, $\Delta E_p$ = 150 mV). In each case, the first oxido-reduction wave ($E_{1/2}^1$) is associated with the oxidation of the ferrocenyl moiety,[18,19,46] with ferrocene/ferrocenium redox potentials cathodically shifted upon complexation of the enaminone core compared to that of the protonated ligand **4**. However, the spin density plots of **$7^+$** and **$8^+$** show fairly large delocalization on the ligand (Fig. S7)[‡] with moderate Fe spin density values (0.50 and

0.47 for $7^+$ and $8^+$, respectively). The Cu spin density remains almost unchanged on going from **8** to $8^+$ (0.45 and 0.48, respectively). The strong electron withdrawing effect of the acyl-type substituent in **4** is partially lost with the formation of the six-membered heterometallacycle.[18a,19b] The second redox wave $(E_{1/2}^2)$ which we attribute to the generation of the doubly oxidized products $7^{2+}$ and $8^{2+}$ at the Pt electrode, is computed to occur both at the iron and M(II) centers, together with additional ONO participation in the case of the more delocalized $7^{2+}$ complex (Fig. S7).[‡] The metal spin densities are 1.10 (Fe) and 0.48 (Ni) in $7^{2+}$ and 1.06 (Fe) and 0.12 (Cu) in $8^{2+}$.
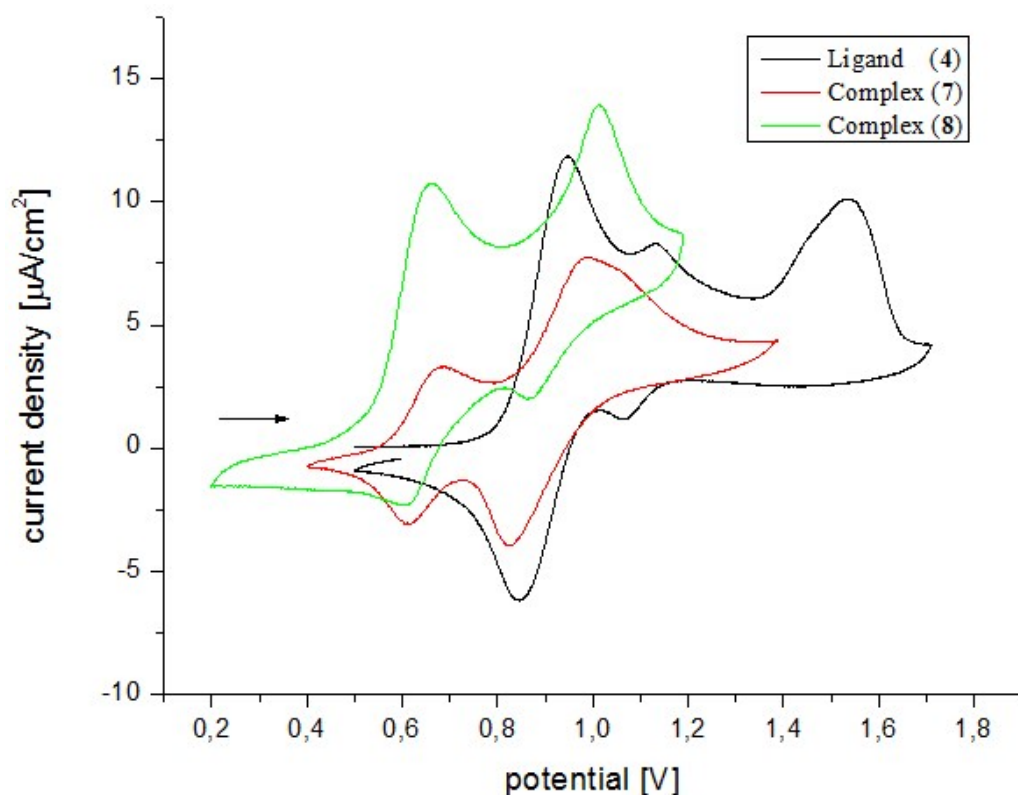


**Fig. 10** Cyclic voltammograms of diprotonated ligand **4** (black line), complex **7** (red line) and complex **8** (green line), recorded in dichloromethane containing 0.1 M $n$-Bu$_4$N$^+$PF$_6^-$ as supporting electrolyte on a Platinum disk working electrode, at 293 K and scan rate = 0.1 Vs$^{-1}$.

## Conclusion

In this contribution, we have synthesized and systematically characterized using FT-IR, NMR and UV-vis absorption spectra, four new four-coordinate square planar nickel(II) and copper(II) based ONO tridentate Schiff base complexes as well as their diprotonated Schiff base precursors resulting from monocondensation of 1-substituted anisyl and ferrocenyl butan-1,3-dione and 2-aminophenol. Reactions of these dianionic tridentate ligands with metal(II) salts in presence of pyridine afforded the desired [(R-ONO)M(py)] complexes. Single crystal X-ray structures have been determined for all the compounds, revealing a noncentrosymmetric packing structure for the [(An-ONO)Ni(py)] derivative **5**. Electronic structural characterization through electrochemical, UV-vis absorption spectroscopy, and computational methods has shown the low-energy optical transition to be HOMO-LUMO in character. All the compounds exhibit second-order NLO responses and the values of $\beta_{1.91}$ measured via the HLS technique in dichloromethane are relatively large for the mononuclear [(An-ONO)M(py)] species **5** and **6** that are very simple structures. This work represents a first step toward the elaboration of extended and more complex push-pull architectures, taking advantage of the lability of the pyridine ancillary ligand. It was very important to demonstrate that these building blocks are able to display relatively high first-order hyperpolarisabilities, in spite of the small extent of conjugated π-electrons. In that prospect, work on new Schiff base building blocks bearing electron withdrawing groups has started.

## Experimental

### General considerations

Manipulations of air-sensitive compounds were carried out under a dry dinitrogen or argon atmosphere using conventional Schlenk techniques. The solvents were dried and distilled according to standard procedures.[52] The compound 1-(4-methoxyphenyl )-1,3-butanedione (**1**)[53] and 1-ferrocenyl-1,3-butanedione (**2**)[19c] ferrocenyl = Fc = CpFe($\eta^5$-C$_5$H$_4$), Cp = $\eta^5$-C$_5$H$_5$) were synthesized according to literature procedures. All other chemicals were purchased from commercial sources and used without further purification. Solid-state IR spectra were recorded on a Perkin-Elmer, Model Spectrum One, FT-IR

spectrophotometer with KBr disks in the 4000 to 400 cm$^{-1}$ range. Electronic spectra were obtained with a Thermo Scientific, Helios Omega, spectrophotometer. The $^1$H and $^{13}$C NMR spectra were measured on either a Bruker AvanceIII 400 or a Bruker Avance 500 Instrument. The chemical shifts ($\delta_H$ and $\delta_C$) were referenced relative to tetramethylsilane (TMS), using the residual solvent resonances of the deuterated solvent used as internal standards and expressed in parts per million (ppm). Coupling constants ($J$) are reported in Hertz (Hz), and integrations are reported as number of protons. The following abbreviations are used to describe peak patterns: br = broad, s = singlet, d = doublet, t = triplet, m = multiplet. $^1$H and $^{13}$C NMR chemical shift assignments are supported by data obtained from $^1$H-$^1$H COSY, $^1$H-$^{13}$C HMQC, and $^1$H-$^{13}$C HMBC NMR experiments, and are given according to the numbering scheme of ORTEPS views (Figs. 1-3). High resolution electro-spray ionization mass spectra (ESI-MS) were acquired on a WATERS Q-TOF II spectrometer at the Centre Régional de Mesures Physiques de l'Ouest (CRMPO, Rennes). Elemental analyses were conducted on a Thermo-FINNIGAN Flash EA 1112 CHNS/O analyzer by the Microanalytical Service of the CRMPO at the University of Rennes 1, France. Cyclic voltammetry (CV) measurements were performed using a Radiometer Analytical model PGZ 100 all-in one potentiostat. A three-electrode cell was used, equipped with a platinum wire auxiliary electrode, a platinum working electrode, and Ag/AgCl as the reference electrode. Dichloromethane solutions were 1.0 mM in the compound under study and 0.1 M in the supporting electrolyte $n$-Bu$_4$N$^+$PF$_6^-$ with voltage scan rate of 100 mVs$^{-1}$. Melting points were determined in evacuated capillaries on a Kofler Bristoline melting point apparatus and were not corrected.

**4-MeO-C$_6$H$_4$-C(O)CH=C(CH$_3$)N(H)-C$_6$H$_4$-2-OH (3).** A three necked round bottom flask equipped with a Dean-Stark apparatus was loaded with a magnetic stir bar, 1-(4-methoxyphenyl)-butane-1,3-dione (**1**) (500 mg, 2.61 mmol), 2-aminophenol (334.5 mg, 3.07 mmol, 1.17 equiv) and 10 mL of toluene. The reaction mixture was refluxed for 2 h. At room temperature (rt), the reaction was monitored by TLC on aluminum plates coated with neutral silica gel (60 F$_{254}$, Merck) with petroleum ether-diethyl ether mixture (1:1) as eluent, to ensure the complete consumption of the starting diketone. Then, 8 mL of diethyl ether were added and the solution stored at -30 °C overnight. The resulting microcrystalline solid formed was collected by filtration, washed with 3 x 2 mL portion of cold petroleum

ether-diethyl ether mixture (1:1), and dried under vacuum. Slow evaporation (5 days) of a solution of the compound in dichloromethane provided 650 mg (2.30 mmol, 88% yield) of colorless microcrystals. A suitable crystal from this crop was used for X-ray structure determination. mp 180-183 °C. Found: C, 72.12; H, 6.10; N, 5.12. $C_{17}H_{17}NO_3$ requires C, 72.07; H, 6.05; N, 4.94%. FT-IR (KBr, cm$^{-1}$): 3150(m) $v$(O-H), 3073(w) $v$(N-H), 3044(w) $v$(C-H aryl), 2928(w) $v$(C-H alkyl), 2844(w) $v_{sym}$(CH$_3$), 1593(s), 1532(m) $v$(C$\cdots$O) and $v$(C$\cdots$C), 1519(s) $\delta$(N-H), 1458(m) $\delta$(O-H), 1257(s) $v_{asym}$(CH$_3$-O-aryl), 1208(m) $v$(C-O), 760(s) $\delta$(C-H). $^1$H NMR (400 MHz, CDCl$_3$, 315 K): $\delta_H$ 1.71 (s, 3 H, CH$_3$), 3.84 (s, 3 H, OCH$_3$), 5.67 (s, 1 H, CH=C), 6.83 (td, $^3J_{H,H}$ = 7.4 and 7.7 Hz, $^4J_{H,H}$ = 1.6 Hz, 1 H, H-4), 6.92 (d, $^3J_{H,H}$ = 9.2 Hz, 2 H, H-13,15), 7.01 (d, $^3J_{H,H}$ = 8.3 Hz, 1 H, H-6), 7.02 (dd, $^3J_{H,H}$ = 7.7 Hz, $^4J_{H,H}$ = 1.6 Hz, 1 H, H-3), 7.15 (ddd, $^3J_{H,H}$ = 7.4 and 8.3 Hz, $^4J_{H,H}$ = 1.6 Hz, 1 H, H-5), 7.85 (d, $^3J_{H,H}$ = 9.0 Hz, 2 H, H-12,16), 12.27 (s, 1 H, NH); OH proton resonance not observed. $^{13}$C{$^1$H} NMR (100 MHz, CDCl$_3$, 315 K): $\delta_C$ 19.89 (CH$_3$), 55.41 (OCH$_3$), 94.30 (C-9), 113.59 (C-13,15), 117.02 (C-6), 120.08 (C-4), 125.59 (C-2), 127.64 (C-3), 128.48 (C-5), 129.25 (C-12,16), 132.72 (C-11), 152.33 (C-1), 162.14 (C-14), 164.21 (C-7), 188.10 (C-10).

**CpFe($\eta^5$-C$_5$H$_4$)-C(O)CH=C(CH$_3$)N(H)-C$_6$H$_4$-2-OH (4).** This organometallic compound was synthesized following a procedure similar to that described above for the organic enaminone **3**, using in this case, 300 mg (1.11 mmol) of ferrocenoylacetone and 121.1 mg (1.11 mmol) of 2-aminophenol in 10 mL of toluene. Recrystallization by slow evaporation (5 days) of a diethyl ether solution of the compound afforded 345 mg (0.96 mmol, 86% yield) of **4** as orange microcrystals. A suitable single crystal from this crop was selected for X-ray structure determination. Mp 95-98 °C. Found: C, 66.44; H, 5.49; N, 3.64. $C_{20}H_{19}FeNO_2$ requires C, 66.50; H, 5.26; N, 3.88%. FT-IR (KBr, cm$^{-1}$): 3427(w) $v_{sym}$(O-H), 3377(m) $v$(N-H), 3088(w) $v$(C-H aryl), 2963(w) $v$(C-H alkyl), 1592(s), 1537(m) $v$(C$\cdots$O) and $v$(C$\cdots$C), 1491(m) $\delta$(N-H), 1445(w) $\delta$(O-H) 752(s) $\delta$(C-H). $^1$H NMR (400 MHz, CDCl$_3$, 298 K): $\delta_H$ 1.73 (s, 3 H, CH$_3$), 4.17 (s, 5 H, C$_5$H$_5$), 4.38 (br t, $^3J_{H,H}$ = 1.8 Hz, 2 H, H$_\alpha$ C$_5$H$_4$), 4.73 (br t, $^3J_{H,H}$ =1.8 Hz, 2 H, H$_\beta$ C$_5$H$_4$), 5.30 (s, 1 H, CH=C), 6.84 (t, $^3J_{H,H}$ = 7.5 Hz, 1 H, H-4), 7.04 and 7.05 (2 x dd, $^3J_{H,H}$ = 7.5 Hz, $^4J_{H,H}$ = 1.1 Hz, 2 x 1 H, H-3 and H-6), 7.16 (br t, $^3J_{H,H}$ = 7.2 Hz, 1 H, H-5), 11.80 (br s, 1 H, NH); OH proton resonance not observed. $^{13}$C{$^1$H} NMR (100 MHz, CDCl$_3$, 298 K): $\delta_C$ 20.05(C-8), 68.64 (C$_\alpha$ C$_5$H$_4$), 69.91

$(C_5H_5)$, 70.95 ($C_\beta$ $C_5H_4$), 82.26 ($C_{ipso}$ $C_5H_4$), 95.80 (C-9), 117.04 (C-6), 119.86 (C-4), 125.79 (C-2), 127.65 (C-3), 128.21 (C-5), 152.44 (C-1), 161.85 (C-7), 193.0 (C-10).

**[{4-MeO-C$_6$H$_4$-C(O)CH=C(CH$_3$)N-C$_6$H$_4$-2-O}Ni(NC$_5$H$_5$)] (5).** A Schlenk tube was charged with a magnetic stir bar, compound **3** (380 mg, 1.05 mmol), potassium *tert*-butoxide (354 mg, 3.16 mmol) and 3 mL of THF. After 5 min of stirring a dark red precipitate formed and the reaction mixture was vigorously stirred for 25 min. Then, 0.25 mL (3.0 mmol) of pyridine was added slowly. After 10 min of stirring, a solution of Ni(NO$_3$)$_2$·6H$_2$O (437 mg, 1.5 mmol) in 1.5 mL of THF was added dropwise and the stirring was continued for 15 min. The reaction mixture was vigorously stirred for 12 h. The reaction was quenched with 5 mL of EtOH giving a light brown precipitate. The solid material was filtered off, washed with 3 x 3 mL portion of cold mixture of THF and EtOH (1:1), diethyl ether (2 x 3 mL portion), and dried under vacuum for 2 h. Slow evaporation (4 days) of a solution of the compound in dichloromethane deposited 318 mg (72% yield) of compound **5** as dark-brown microcrystals. A suitable monocrystal from this crop was used for X-ray structure determination. Mp 170-172 °C. Found: C, 62.30; H, 4.63; N, 6.50. C$_{22}$H$_{22}$NiN$_2$O$_3$ requires C, 62.75; H, 5.27; N, 6.65%. FT-IR (KBr, cm$^{-1}$): 3049(w) $\nu$(C-H aryl), 2932(w) $\nu$(C-H alkyl), 2832(w) $\nu_{sym}$(CH$_3$), 1604(s) $\nu$(C⋯O), $\nu$(C⋯N) and/or $\nu$(C⋯C), 1557(s), 1244(s) $\nu_{asym}$(CH$_3$-O-aryl), 764(s) $\delta$(C-H). $^1$H NMR (400 MHz, CD$_2$Cl$_2$, 298 K): $\delta_H$ 2.61(s, 3 H, CH$_3$), 3.85 (s, 3 H, OCH$_3$), 5.97 (s, 1 H, H-9), 6.44 (t, $^3J_{H,H}$ = 7.3 Hz, 1 H, H-4), 6.64 (d, $^3J_{H,H}$ = 7.3 Hz, 1 H, H-6), 6.81 (t, $^3J_{H,H}$ = 7.3 Hz, 1 H, H-5), 6.88 (d, $^3J_{H,H}$ = 8.8 Hz, 2 H, H-13 and 15), 7.37 (d, $^3J_{H,H}$ = 8.0 Hz, 1 H, H-3), 7.46 (br s, 2 H, H-19 and 21), 7.61 (d, $^3J_{H,H}$ = 8.8 Hz, 2 H, H-12 and 16), 7.88 (t, $^3J_{H,H}$ = 7.4 Hz, 1 H, H-20), 8.73 (br s, 2 H, H-18 and 22). $^{13}$C{$^1$H} NMR (100 MHz, CD$_2$Cl$_2$, 298 K): $\delta_C$ 25.25 (CH$_3$), 55.28 (OCH$_3$), 101.00 (C-9), 113.11 (C-4), 113.47 (C-13 and 15), 115.70 (C-6), 121.10 (C-3), 124.01 (C-19 and 21),124.74 (C-5), 127.95 (C-12 and 16), 129.71 (C-11), 138.01 (C-20), 142.50 (C-2), 150.30 (C-18 and 22), 160.96 (C-14), 161.85 (C-7), 164.56 (C-1), 168.72 (C-10).

**[{4-MeO-C$_6$H$_4$-C(O)CH=C(CH$_3$)N-C$_6$H$_4$-2-O}Cu(NC$_5$H$_4$-4-CMe$_3$] (6).**[23] This known complex, albeit previously prepared using a slightly different *modus operandi*, was synthesized following a procedure similar to that described for complex **5** using, in this case, **3** (350 mg, 1.24 mmol), potassium *tert*-butoxide (416 mg, 3.72 mmol), 3.5 mL of

THF, 0.44 mL (3.0 mmol) of 4-*tert*-butylpyridine and a solution of $Cu(NO_3)_2 \cdot 3H_2O$ (300 mg, 1.24 mmol) in 1.5 mL of THF. Yield: 506 mg (75%) of a dark-green microcrystalline solid. Compound **6** was identified by comparison of its melting point and FT-IR spectral data with those of an authentic sample.[23]

**[{CpFe($\eta^5$-C$_5$H$_4$)-C(O)CH=C(CH$_3$)N-C$_6$H$_4$-2-O}Ni(NC$_5$H$_5$)] (7).** The synthesis of this complex was carried out following a procedure similar to that described for complex **5** using, in this case, **4** (380 mg, 1.05 mmol), potassium *tert*-butoxide (354 mg, 3.16 mmol), 3 mL of THF, 0.25 mL (3.0 mmol) of pyridine and a solution of $Ni(NO_3)_2 \cdot 6H_2O$ (437 mg, 1.5 mmol) in 1.5 mL of THF. Yield: 390.7 mg (75%) of orange microcrystals that were isolated upon slow evaporation (5 days) of a solution of the compound in dichloromethane. A suitable crystal from this crop was used for X-ray structure determination. Mp 168-170 °C. Found: C, 60.37; H, 4.53; N, 5.49. $C_{25}H_{22}FeN_2NiO_2$ requires C, 60.42; H, 4.46; N, 5.64%. ESI MS (m/z), calcd for $C_{25}H_{22}N_2O_2{}^{56}Fe^{58}Ni$: 496.03841, found: 496.0385 (0 ppm) [M$^+$]. FT-IR (KBr, cm$^{-1}$): 3118-3080(w) $v$(C-H aryl), 2926(w) $v$(C-H alkyl), 1606(m) $v$(C$\cdots$O), $v$(C$\cdots$N) and/or $v$(C$\cdots$C), 1562(s), 1504(m)-1408(s) $v$(C$\cdots$C) py, 754(s) $\delta$(C-H). $^1$H NMR (500 MHz, CD$_2$Cl$_2$, 253 K): $\delta_H$ 2.49 (s, 3 H, CH$_3$), 4.15 (s, 5 H, C$_5$H$_5$), 4.28 (br s, 2 H, H$_\beta$ C$_5$H$_4$), 4.50 (br s, 2 H, H$_\alpha$ C$_5$H$_4$), 5.60 (s, 1 H, H-9), 6.39 (t, $^3J_{H,H}$ = 7.8 Hz, 1 H, H-4), 6.64 (d, $^3J_{H,H}$ = 7.9 Hz, 1 H, H-6), 6.75 (t, $^3J_{H,H}$ = 7.5 Hz, 1 H, H-5), 7.29(d, $^3J_{H,H}$ = 7.3 Hz, 1 H, H-3), 7.45 (t, $^3J_{H,H}$ = 6.3 Hz, 2 H, H-22 and 24), 7.86 (t, $^3J_{H,H}$ = 7.6 Hz, 1 H, H-23), 8.62 (d, $^3J_{H,H}$ = 4.6 Hz, 2 H, H-21 and 25). $^{13}$C{$^1$H} NMR (125 MHz, CD$_2$Cl$_2$, 298 K): $\delta_C$ 25.31 (CH$_3$), 67.62 (C$_\alpha$ C$_5$H$_4$), 69.72 (C$_5$H$_5$), 70.05 (C$_\beta$ C$_5$H$_4$), 81.31 (C$_{ipso}$ C$_5$H$_4$), 101.26 (C-9), 113.12 (C-4), 115.84 (C-6), 120.13 (C-3), 124.44 (C-5), 142.72 (C-2), 160.70 (C-7), 164.07 (C-1), 172.92 (C-10); NC$_5$H$_5$ not observed.

**[{CpFe($\eta^5$-C$_5$H$_4$)-C(O)CH=C(CH$_3$)N-C$_6$H$_4$-2-O}Cu(NC$_5$H$_5$)] (8).** This complex was synthesized following a similar procedure to that described for complex **5** using, in this case, **4** (380 mg, 1.05 mmol), potassium *tert*-butoxide (354 mg, 3.16 mmol), 3 mL of THF, 0.25 mL (3.0 mmol) of pyridine and a solution of $Cu(NO_3)_2 \cdot 3H_2O$ (362.4 mg, 1.5 mmol) in 1.5 mL of THF. Slow evaporation (4 days) of a solution of the compound in dichloromethane deposited 368.9 mg (70% yield) of **8** as dark-brown microcrystals. A suitable monocrystal from this crop was used for X-ray structure determination. mp 163-166 °C. Found: C, 59.56; H, 4.22; N, 5.61. $C_{25}O_2H_{22}N_2FeCu$ requires C, 59.83; H, 4.42; N,

5.58%. ESI MS (m/z), calcd for $C_{25}H_{22}N_2O_2{}^{56}Fe^{63}Cu$: 501,03267, found: 501.0330 (1 ppm) [$M^+$]. FT-IR (KBr, $cm^{-1}$): 3111-3050(w) $v$(C-H aryl), 1607(w) $v$(C⋯O), $v$(C⋯N) and/or $v$(C⋯C), 1567(s), 1504(m)-1412(s) $v$(C⋯C py), 753(s) $\delta$(C-H).

### X-ray crystal structure determinations

A crystal of appropriate size and shape of compounds **3**, **4**, **5**, **7** and **8** was coated in Paratone-N oil, mounted on a cryoloop and transferred to the cold gas stream of the cooling device. Intensity data were collected at $T$ = 150(2) K on a Bruker APEXII AXS diffractometer using Mo-Kα radiation (λ = 0.71073 Å), equipped with a bidimensional CCD detector, and were corrected for absorption effects using multiscanned reflections. All structures were solved by direct methods using the *SIR97* program,[54] and then refined with full-matrix least-square methods based on $F^2$ (*SHELXL-97*),[55] with the aid of the *WINGX* program.[56] In 3, the H(1) atom was found in Fourier difference maps and refined. The disorder observed for the oxygen atom of the *o*-phenol rings was modelled using two positions with fixed 0.50 and 0.50 occupancy factors for each oxygen. For **4**, the contribution of the disordered solvents to the calculated structure factors was estimated following the *BYPASS* algorithm,[57] implemented as the *SQUEEZE* option in *PLATON*.[58] A new data set, free of solvent contribution, was then used in the final refinement. The disorder observed for the carbon atoms of the free cyclopentadienyl ring of the third crystallographically independent molecule **4C** was modelled using two positions per carbon with fixed 0.50 and 0.50 occupancy factors for each carbon. All non-hydrogen atoms were refined with anisotropic atomic displacement parameters. Hydrogen atoms were placed in their geometrically idealized positions and constrained to ride on their parent atoms. A summary of the details about the data collection and refinement for the X-ray structures of the five compounds are documented in Table 4, and additional crystallographic details are in the CIF files (ESI).‡ ORTEP views were drawn using *OLEX2* software.[59]

**Table 4** Crystallographic data, details of data collection and structure refinement parameters for compounds **3**, **4**, **5**, **7** and **8**

| | 3 | 4 | 5 | 7 | 8 |
|---|---|---|---|---|---|
| Empirical formula | $C_{17} H_{17} N O_3$ | $C_{60} H_{54} Fe_3 N_3 O_6$ | $C_{44} H_{40} N_4 Ni_2 O_6$ | $C_{25} H_{22} Fe N_2 Ni O_2$ | $C_{50} H_{44} Cu_2 Fe_2 N_4 O_4$ |
| Formula weight | 283.32 | 1080.61 | 838.22 | 497.01 | 1003.67 |
| Collection T (K) | 150(2) | 150(2) | 150(2) | 150(2) | 150(2) |
| Crystal size (mm) | 0.43 x 0.33 x 0.18 | 0.54 x 0.37 x 0.23 | 0.58 x 0.15 x 0.06 | 0.50 x 0.08 x 0.03 | 0.40 x 0.35 x 0.09 |
| Crystal system | tetragonal | triclinic | orthorhombic | orthorhombic | monoclinic |
| space group | $P\text{-}4\,2_1\,c$ | $P\text{-}1$ | $P2_1\,2_1\,2_1$ | *Pc a b* | *P2₁/a* |
| a (Å) | 19.8481(7) | 14.3007(7) | 7.2819(2) | 7.5236(5) | 7.5792(5) |
| b (Å) | 19.8481(7) | 14.7917(6) | 21.2966(6) | 22.6943(12) | 23.0612(13) |
| c (Å) | 7.1359(3) | 15.2273(6) | 23.7759(7) | 23.9482(15) | 23.4845(15) |
| α (°) | 90 | 95.987(2) | 90 | 90 | 90 |
| β (°) | 90 | 109.006(2) | 90 | 90 | 90.527 |
| γ (°) | 90 | 105.734(2) | 90 | 90 | 90 |
| Z | 8 | 2 | 4 | 8 | 4 |
| $D_{calcd}$ (g.cm$^{-3}$) | 1.339 | 1.253 | 1.510 | 1.615 | 1.624 |
| V (Å$^3$) | 2811.17(15) | 2864.9(2) | 3687.16(18) | 4089.0(4) | 4104.6(4) |
| Abs. coeff. (mm$^{-1}$) | 0.092 | 0.799 | 1.079 | 1.656 | 1.769 |
| F(000) | 1200 | 1122 | 1744 | 2048 | 2056 |
| θ range (°) | 3.52 to 27.48 | 2.93 to 27.48 | 2.93 to 27.45 | 2.98 to 27.48 | 2.95 to 27.75 |
| range h, k ,l | -25/19, -18/25, -6/9 | -18/18, -19/17, -17/19 | -8/9, -26/27, -27/30 | -9/9, -28/29, -31/23 | -9/9, -29/29, -30/29 |
| No. Refl. collected | 11631 | 41885 | 32926 | 18668 | 34974 |
| No. Indepent Refl. | 1825 [R(int) = 0.0429] | 12931 [R(int) = 0.0498] | 8401 [R(int) = 0.0503] | 4653 [R(int) = 0.0668] | 34974 [R(int) = 0.00] |
| Comp. to $θ_{max}$ (%) | 99.5 | 98.5 | 99.6 | 99.4 | 99.5 (θ = 25.0°) |
| Max/min transmission | 0.984/0.841 | 0.832/0.694 | 0.937/0.777 | 0.952/0.760 | 0.853/0.660 |
| Data / restraints / parameters | 1825/0/197 | 12931/0/619 | 8401/0/509 | 4653/0/281 | 34974/0/562 |
| Final R indices [I>2σ(I)] | $R_1 = 0.0762$ $wR_2 = 0.1605$ | $R_1 = 0.0569$ $wR_2 = 0.1537$ | $R_1 = 0.0368$ $wR_2 = 0.064$ | $R_1 = 0.0449$ $wR_2 = 0.0947$ | $R_1 = 0.0591$ $wR_2 = 0.1436$ |
| R indices (all data) | $R_1 = 0.0827$ $wR_2 = 0.1635$ | $R_1 = 0.0824$ $wR_2 = 0.165$ | $R_1 = 0.0496$ $wR_2 = 0.0676$ | $R_1 = 0.0841$ $wR_2 = 0.1097$ | $R_1 = 0.0763$ $wR_2 = 0.159$ |
| Goodness-of-fit on (F$^2$) | 1.273 | 1.088 | 1.049 | 1.088 | 1.036 |
| Largest diff. peak/hole (e A$^{-3}$) | 0.332/-0.355 | 1.795/-1.075 | 0.457/-0.367 | 0.567/-0.651 | 1.06 /-1.206 |

### HLS measurements

The first order hyperpolarizabilities $β_{1.91}$ of compounds **3-8** were acquired using the HLS technique[60] at 1.91 μm. The measurements were carried out with $10^{-2}$ M solutions in

dichloromethane following a well-established procedure.[18,22] Ethyl violet 1.0 x $10^{-2}$ M in dichloromethane was used as reference, its octupolar $\beta$ value being 170 x $10^{-30}$ esu at 1.91 μm.[61]

### Computational details

DFT calculations[62] were carried out using the Amsterdam Density Functional (ADF2012) program.[63] Geometry optimizations were performed with the PW91 functional[64] and the standard TZ2P basis set[65] was used in all the calculations.[62] The frozen-core approximation was used to treat the core shells up to 1s for C, N and O, and up to 3p for Fe, Ni and Cu.[62] Spin-unrestricted calculations were carried out on the odd-electrons systems. The optimized geometries of all species were characterized as true minima on their potential energy surfaces using vibrational frequency calculations. In the case of complex **6**, the simplified model **6'**, in which the *tert*-Butyl group was replaced by hydrogen, was considered. For each compound, calculations have been performed considering the isolated molecule (vacuum state) as well as applying solvent ($CH_2Cl_2$) effect corrections using the Conductor like Screening Model (COSMO)[66] included in the ADF package. The TD-DFT[67] method implemented in the ADF package was applied to calculate the UV-vis electronic absorption transitions on the PW91-optimized geometries, using the hybrid B3LYP functional,[68] and with and without solvent ($CH_2Cl_2$) COSMO corrections. UV-vis spectra were simulated from the computed TD-DFT transitions and their oscillator strengths by using the SWizard program,[69] each transition being associated with a Gaussian function of half-height width equal to 3000 $cm^{-1}$. The optimized geometries were drawn using the MOLDEN program.[70]

### Acknowledgements

## Notes and references

‡ Electronic supplementary information (ESI) available: VT ^{1}H NMR of **7** (Fig. S1), packing diagrams of **3** and **4** (Fig. S2), experimental UV-Vis spectra of **3-8** (Fig. S3), optimized geometries of **3-8** (Fig. S4), molecular orbital diagrams of **6'** (Fig. S5) and of **8** (Fig. S6), spin density plot of **3-8** (Fig. S7), experimental and computed IR frequencies of **3-8** (Table S1), selected bond lengths and angles with their theoretically computed values for **3**, **4**, **5-8** (Tables S2-S4), metrical parameters of Fc in **4**, **7** and **8** (Table S5), hydrogen bonds in **3** and **4** (Table S6), comparison of enaminone core bond distances of **3-8** (Table S7), crystallographic data for structural analysis (in CIF format), and Cartesian coordinates of all the optimized structures.CCDC 1058274-1058278. For ESI and crystallographic data in CIF or other electronic format see DOI:

1   (*a*) E. Goovaerts, W. E. Wenseleers, M. H. Garcia and G. H. Cross, in *Handbook of Advanced Electronic and Photonic Materials and Devices*, Ed. H. S. Nalwa, *Nonlinear Optical Materials*, Academic Press, New York, 2001, Vol. 9, pp. 127; (*b*) *Handbook of Optics IV, Fiber Optics & Nonlinear Optics*, Eds. M. Bass, J. M. Enoch, E. W. van Stryland and W. L. Wolfe, 2nd edn, McGraw-Hill, New York, 2001.

2   For reviews, see: (*a*) M. Liang and J. Chen, *Chem. Soc. Rev.*, 2013, **42**, 3453-3488; (*b*) A. C. Grimsdale, K. L. Cahn, R. E. Martin, P. G. Jokisz and A. B. Holmes, *Chem. Rev.*, 2009, **109**, 897-1091.

3   (*a*) N. P. Prasad and D. J. Williams, *Introduction to Nonlinear Optical Effects in molecules and Polymers*, Wiley, New York, 1991; (*b*) J. Zyss, *Molecular Nonlinear Optics: Materials, Physics and Devices*, Academic Press, Boston, 1994; (*c*) *Nonlinear Optical Properties of Matter: From Molecules to Condensed Phases*, Eds. M. G. Papadopoulos, J. Leszczynski and A. J. Sadlej, Springer, Dordrecht, 2006.

4   (*a*) L. T. Cheng, W. Tam, S. H. Stevenson, G. R. Meredith, G. Rikken and S. R. Marder, *J. Phys. Chem.,* 1991, **95**, 10631-10643; (*b*) L. T. Cheng, W. Tam, S. R. Marder, A. E. Stiegman, G. Rikken and C. W. Spangler, *J. Phys. Chem.*, 1991, **95**, 10643-10652.

5   (*a*) *Nonlinear Optics of Organic Molecules and Polymers*, Eds. H. S. Nalwa and S. Miyata, CRC Press, Boca Raton, FL, 1997; (*b*) *Nonlinear Optical Properties of*

*Organic Molecules and Crystals*, Eds. D. S. Chemla and J. Zyss, Academic Press, Orlando, 1987, Vols. 1 and 2; (*c*) M. Bhattacharya, P.K. Das and A.G. Samuelson, *Handbook of Organic Electronics and Photonics*, Ed. H.S. Nalwa, American Scientific Pub, California, USA, 2007, vol. 2, pp. 109-147; (*d*) F. Bures, *RSC Adv.*, 2014, **4**, 58826-58851; (*e*) W. Wu, R. Tang, Q. Li and Z. Li, *Chem. Soc. Rev.*, 2015, **44**, DOI: 10.1039/c4cs00224e.

6   For very recent examples, see: (*a*) M. Shimada, Y. Yamanoi, T. Matsushita, T. Kondo, E. Nishibori, A. Hatakeyama, K. Sugimoto and H. Nishihara, *J. Am. Chem. Soc.*, 2015, **137**, 1024-1027; (*b*) H. M. Heitzer, T. J. Marks and M. A. Ratner, *J. Am. Chem. Soc.*, 2015, **137**, 7189-7196; (c) H. Wang, F. Liu, Y. Yang, M. Zhang, C. Peng, S. Bo, X. Liu, L. Qiu and Z. Zhen, *New J. Chem.*, 2015, **39**, 1038-1044; (d) S. Achelle, S. Kahlal, A. Barsella, J.-Y. Saillard, X. Che, J. Vallet, F. Bureš, B. Caro and F. Robin-le Guen, *Dyes Pigm.*, 2015, **113**, 562-570; (e) S. Achelle, J. P. Malval, S. Aloïse, A. Barsella, A. Spangenberg, L. Mager, H. Akdas-Kilig, J. L. Fillaut, B. Caro and F. Robin-le Guen, *ChemPhysChem*, 2013, **14**, 2725-2736.

7   (*a*) M. G. Humphrey, T. Schwich, P. J. West and M. P. Cifuentes, M. Samoc, in *Comprehensive Inorganic Chemistry II*, eds. J. Reedijk and K. Poeppelmeier, Elsevier, Oxford, 2013, Vol. 8, pp. 781-835; (*b*) O. Maury and H. Le Bozec, in *Molecular Materials*, Eds. D. W. Bruce, D. O'Hare and R. I. Walton, Wiley, Chichester, 2010, pp. 1-59; (*c*) M. E. Thompson, P. E. Djurovich, S. Barlow and S. R. Marder, in *Comprehensive Organometallic Chemistry III*, Vol. Ed. D. O'Hare, Series Eds. R. H. Crabtree and D. M. P. Mingos, Elsevier, Oxford, 2006, Vol. 12, pp. 101; (*d*) B. J. Coe, in *Comprehensive Coordination Chemistry II*, Eds. J. A. McCleverty and T. J. Meyer, Elsevier Pergamon, Oxford, 2004, Vol. 9, pp. 621-687.

8   Selected review articles and cited references: (*a*) B. J. Coe, *Coord. Chem. Rev.*, 2013, **257**, 1438-1458; (*b*) S. Di Bella, C. Dragonetti, M. Pizzotti, D. Roberto, F. Tessore and R. Ugo, *Top. Organomet. Chem.*, 2010, **28**, 1-55; (*c*) J. P. Morrall, G. T. Dalton, M. G. Humphrey and M. Samoc, *Adv. Organomet. Chem.*, 2008, **55**, 61-136; (*d*) B. J. Coe, *Acc. Chem. Res.*, 2006, **39**, 383-393; (*e*) E. Cariati, M. Pizzotti, D. Roberto, F. Tessore and R. Ugo, *Coord. Chem. Rev.*, 2006, **250**, 1210- 1233; (*f*) O. Maury and H. Le

Bozec, *Acc. Chem. Res.*, 2005, **38**, 691-704; (*g*) C. E. Powell and M. G. Humphrey, *Coord. Chem. Rev.*, 2004, **248**, 725-756. (*h*) S. Di Bella, *Chem. Soc. Rev.*, 2001, **30**, 355-366 .

9    Selected recent inorganic examples: (*a*) J. Boixel, V. Guerchais, H. Le Bozec, D. Jacquemin, A. Amar, A. Boucekkine, A. Colombo, C. Dragonetti, D. Marinotto, D. Roberto, S. Righetto and R. De Angeli, *J. Am. Chem. Soc.*, 2014, **136**, 5367-5375; (*b*) B. J. Coe, S. P. Foxon, R. A. Pilkington, S. Sánchez, D. Whittaker, K. Clays, G. Depotter and B. S. Brunschwig, *Organometallics*, 2015, **34**, 1701-1715; (*c*) B. J. Coe, M. Helliwell, M. K. Peers, J. Raftery, D. Rusanova, K. Clays, G. Depotter and B. S. Brunschwig, *Inorg. Chem.*, 2014, **53**, 3798-3811; (*d*) L. Pilia, M. Pizzotti, F. Tessore and N. Robertson, *Inorg. Chem.*, 2014, **53**, 4517-4526; (*e*) M. M. Ayhan, A. Singh, E. Jeanneau, V. Ahsen, J. Zyss, I. Ledoux-Rak, A. G. Gurek,† C. Hirel, Y. Bretonnière and C. Andraud, *Inorg. Chem.*, 2014, **53**, 4359-4370; (*f*) P. Xie, L. Wang, Z. Huang, F. Guo and Q. Jin, *Eur. J. Inorg. Chem.*, 2014, 2544-2551; (*g*) C. Zúñiga, I. Crivelli and B. Loeb, *Polyhedron*, 2015, **85**, 511-518.

10   Selected recent organometallic examples: (*a*) F. Nisic, A. Colombo, C. Dragonetti, E. Garoni, D. Marinotto, S. Righetto, F. De Angelis, M. G. Lobello, P. Salvatori, P. Biagini and F. Melchiorre, *Organometallics*, 2015, **34**, 94-104; (*b*) Y. Shi, G. Li, B. Zhao, Y. Chen, P. Chao, H. Zhang, X. Wang and T. Wang, *Inorg. Chim. Acta*, 2015, **427**, 259-265; (*c*) S. De, R. Mitra, A.G. Samuelson and P. K. Das, *J. Organomet. Chem.*, 2015, **785**, 72-76; (*d*) E. A. Ziemann, S. Baljak, S. Steffens, T. Stein, N. Van Steerteghem, I. Asselberghs, K. Clays and J. Heck, *Organometallics*, 2015, **34**, 1692-1700; (*e*) T. J. L. Silva, P. J. Mendes, A. M. Santos, M. H. Garcia, M. P. Robalo, J. P. P. Ramalho, A. J. P. Carvalho, M. Büchert, C. Wittenburg and J. Heck, *Organometallics*, 2014, **33**, 4655-4671.

11   Review articles and cited references: (*a*) C. R. Nayar and R. Ravikumar, *J. Coord. Chem.*, 2014, **67**, 1-16; (*b*) P. G. Lacroix, *Eur. J. Inorg. Chem.*, 2001, 339-348; (*c*) S. Di Bella and I. Fragalà, *Synth. Met.*, 2000, **115**, 191-196.

12   Selected examples: (*a*) B. M. Muñoz-Flores, R. Santillán, N. Farfán, V. Álvarez-Venicio, V. M. Jiménez-Pérez, M. Rodríguez, O. G. Morales-Saavedra, P. G. Lacroix,

C. Lepetit and K. Nakatani, *J. Organomet. Chem.*, 2014, **769**, 64-71; (*b*) J. M. Rivera, D. Guzman, M. Rodriguez, J. F. Lamere, K. Nakatani, R. Santillan, P. G. Lacroix and N. Farfan, *J. Organomet. Chem.*, 2006, **691**, 1722-1732; (*c*) J.-P. Costes, J. F. Lamere, C. Lepetit, P. G. Lacroix and F. Dahan, *Inorg. Chem.*, 2005, **44**, 1973-1982; (*d*) O. Margeat, P. G. Lacroix, J. P. Costes, B. Donnadieu and C. Lepetit, *Inorg. Chem.*, 2004, **43**, 4743-4750.

13   Selected examples: (*a*) S. Righetto and S. Di Bella, *Dalton Trans.*, 2014, **43**, 2168-2175; (*b*) L. Rigamonti, F. Demartin, A. Forni, S. Righetto and A. Pasini, *Inorg. Chem.*, 2006, **45**, 10976-10989; (*c*) J. Gradinaru, A. Forni, V. Druta, F. Tessore, S. Zecchin, S. Quici and N. Garbalau, *Inorg. Chem.*, 2007, **46**, 884-895; (*d*) S. di Bella, I. Fragala, A. Guerri, P. Dapporto and K. Nakatani, *Inorg. Chim. Acta*, 2004, **357**, 1161-1167; (*e*) F. Cariati, U. Caruso, R. Centore, W. Marcolli, A. De Maria, B. Panunzi, A. Roviello and A. Tuzi, *Inorg. Chem.*, 2002, **41**, 6597-6603.

14   Traditionally, the term salen refers to ligands prepared via the condensation of salicylaldehyde and ethylenediamine, but has come to include dianionic $N_2O_2$ ligands with varying carbonyl-containing substituents and diamine backbones.

15   (*a*) S. di Bella, I. Fragala, I. Ledoux and T. J. Marks, *J. Am. Chem. Soc.*, 1995, **117**, 9481-9485; (*b*) S. di Bella, I. Fragala, I. Ledoux, M. A. Díaz-García and T. J. Marks, *J. Am. Chem. Soc.*, 1997, **119**, 9550.

16   Hernandez- . Molina and A. RMederos, in *Comprehensive Coordination Chemistry II*, Eds. J.A. McCleverty and T. J. Meyer, Elsevier Pergamon, Oxford, 2004, vol. 1, pp. 411-458.

17   (*a*) J.-P. Costes, *Polyhedron*, 1987, **6**, 2169-2175 and references cited; (*b*) S. Chattopadhyay, M. Sinha and S. Chaudhuri, *Inorg. Chim. Acta*, 2006, **359**, 1367-1375.

18   (*a*) A. Trujillo, M. Fuentealba, D. Carrillo, C. Manzur, I. Ledoux-Rak, J.-R. Hamon and J.-Y. Saillard, *Inorg. Chem.*, 2010, **49**, 2750-2764; (*b*) J. Cisterna, V. Dorcet, C. Manzur, I. Ledoux-Rak, J.-R. Hamon and D. Carrillo, *Inorg. Chim . Acta*, 2015, **430**, 82-90.

19  (*a*) A. Trujillo, F. Justaud, L. Toupet, O. Cador, D. Carrillo, C. Manzur and J.-R. Hamon, *New J. Chem.*, 2011, **35**, 2027-2036; (*b*) A. Trujillo, S. Sinbandhit, L. Toupet, D. Carrillo, C. Manzur and J.-R. Hamon, *J. Inorg. Organomet. Polym. Mater.*, 2008, **18**, 81-99; (*c*) M. Fuentealba, J.-R. Hamon, D. Carrillo and C. Manzur, *New J. Chem.*, 2007, **31**, 1815-1825.

20  (*a*) M. Fuentealba, A. Trujillo, J.-R. Hamon, D. Carrillo and C. Manzur, *J. Mol. Struct.*, 2008, 881, 76-82; (*b*) P. Hu, L. Zhang, X. Zhu, X. Liu, L. Ji and Y. Chen, *Polyhedron*, 1989, **8**, 2459-2462.

21  S. Celedon, M. Fuentealba, T. Roisnel, J.-R. Hamon, D. Carrillo and C. Manzur, *Inorg. Chim. Acta*, 2012, **390**, 184-189.

22  S. Celedón, V. Dorcet, T. Roisnel, A. Singh, I. Ledoux-Rak, J.-R. Hamon, D. Carrillo and C. Manzur, *Eur. J. Inorg. Chem.*, 2014, 4984-4993.

23  N. Novoa, F. Justaud, P. Hamon, T. Roisnel, O. Cador, B. Le Guennic, C. Manzur, D. Carrillo and J.-R. Hamon, *Polyhedron*, 2015, **86**, 81-88.

24  (*a*) P. P. Chakrabarty, S. Giri, D. Schollmeyer, H. Sakiyama, M. Mikuriya, A. Sarkar and S. Saha, *Polyhedron*, 2015, **89**, 49-54; (*b*) R. Takjoo, A. Akbari, S. Y. Ebrahimipour, H. A. Rrudbari and G. Brunò, *C. R. Chimie*, 2014, **17**, 1144-1153; (*c*) L. Rigamonti, A. Forni, R. Pievo, J. Reedijk and A. Pasini, *Inorg. Chim. Acta*, 2012, **387**, 373-382; (*d*) L. Rigamonti, A. Forni, R. Pievo, J. Reedijk and A. Pasini, *Dalton Trans.*, 2011, **40**, 3381-3393; (*e*) L. Rigamonti, A. Cinti, A. Forni, A. Pasini and O. Piovesana, *Eur. J. Inorg. Chem.*, 2008, 3633-3647; (*f*) Q. L. Zhang and B. X. Zhu, *J. Coord. Chem.*, 2008, **61**, 2340-2346; (*g*) R.N. Patel, V.L.N. Gundla and D.K. Patel, *Polyhedron*, 2008, **27**, 1054-1060.

25  (*a*) J. M. Rivera, D. Guzmán, M. Rodríguez, J. F. Lamére, K. Nakatani, R. Santillan, P. G. Lacroix and N Farfán, *J. Organomet. Chem.*, 2006, **691**, 1722-1732; (*b*) J. M. Rivera, H. Reyes, A. Cortés, R. Santillan, P. G. Lacroix, C. Lepetit, K. Nakatani and N. Farfán, *Chem. Mater.*, 2006, **18**, 1174-1183.

26  F. Borbone, U. Caruso, R. Centore, A. De Maria, A. Fort, M. Fusco, B. Panunzi, A. Roviello and A. Tuzi, *Eur. J. Inorg. Chem.*, 2004, 2467-2476.

27  (*a*) J.-P. Costes, J. F. Lamère, C. Lepetit, P. G. Lacroix, F. Dahan and K. Nakatani, *Inorg. Chem.*, 2005, **44**, 1973-1982; (*b*) F. Averseng, P. G. Lacroix, I. Malfant, G. Lenoble, P. Cassoux, K. Nakatani, I. Maltey-Fanton, J. A. Delaire and A. Aukauloo, *Chem. Mater.*, 1999, **11**, 995-1002.

28  (*a*) C.-G. Liu, Y.-Q. Qiu, S.-L. Sun, N. Li, G.-C. Yang and Z.-M. Su, *Chem. Phys. Lett.*, 2007, **443**, 163-168; (*b*) C.-G. Liu, Y.-Q. Qiu, S.-L. Sun, H. Chen, N. Li, Z.-M. Su, *Chem.Phys. Lett.*, 2006, **429**, 570-574.

29  M. G. Kuzyk, *Quantum limits of the hyper-Rayleigh scattering susceptibility*, *IEEE Journal on Selected Topics in Quantum Electronics*, 2001, **7**, 774 -780.].

30  (*a*) J. V. Greenhill, *Chem. Soc. Rev.*, 1977, **6**, 277-294; (*b*) C.-H. Lin, H. Pan, V. N. Nesterov and M. G. Richmond, *J. Organomet. Chem.*, 2013, **748**, 56-62; (*c*) M. A. Gaona, F. Montilla, E. Álvarez and A. Galindo, *Dalton Trans.*, 2015, **44**, 6516-6525.

31  (*a*) Y.-C. Shi, H.-M. Yang, W.-B. Shen, C.-G. Yan and X.-Y. Hu, *Polyhedron*, 2004, **23**, 15-21; (*b*) Y.-C. Shi, H.-M. Yang, W.-B. Shen, C.-G. Yan and X.-Y. Hu, *Polyhedron*, 2004, **23**, 1541-1546; (*c*) Y.-C. Shi, C.-X. Sui, H.-B. Song and P.-M. Jian, *J. Coord. Chem.*, 2005, **58**, 363-371; (*d*) Y.-C. Shi, H.-J. Cheng and S.-H. Zhang, *Polyhedron*, 2008, **27**, 3331-3336.

32  J. D. Dunitz, L. E. Orgel and A. Rich, *Acta Crystallogr.*, 1956, **9**, 373-375.

33  Such R-C(=O)CH=C-(R')N(H)R'' derivatives may have the following four isomers: *E-s-E*, *E-s-Z*, *Z-s-E*, and *Z-s-Z* in which *E* and *Z* refer to two possible geometric conformations for the carbon-carbon double bond and *s-E* and *s-Z* to both isomerisms about the carbon-carbon single bond between the carbon-carbon and carbon-oxygen double bonds; see references 29.

34  P. Gilli, V. Bertolasi, V. Ferretti and G. Gilli, *J. Am. Chem. Soc.*, 2000, **122** , 10405-10417.

35  F.H. Allen, O. Kennard, D.G. Watson, L. Brammer, A.G. Orpen and R. Taylor, *J. Chem. Soc., Perkin Trans.*, 1987, S1-S19.

36   (*a*) Y.-C. Shi, S.-H. Zhang, H.-J. Cheng and W.-P. Sun, *Acta Crystallogr., Sect. C: Cryst. Struct. Commun.*, 2006, **62**, m407-m410; (*b*) Y.-C. Shi, *Acta Crystallogr., Sect. E: Struct. Rep. Online,* 2005, **61**, m811-m812.

37   The ionic radii of Ni(II) and Cu(II) metal ions are of 0.63 and 0.71 Å, respectively. F. A. Cotton, G. Wilkinson, C. A. Murillo and M. Bochmann, *Advanced Inorganic Chemistry,* Sixth Edn, Wiley & sons, New York, 1999, pp. 1303–1304.

38   J.L. Oudar, *J. Chem. Phys.*, 1977, **67**, 446-457.

39   (*a*) A. Krishnan, S. K. Pal, P. Nandakumar, A. G. Samuelson and P. K. Das, *Chem. Phys.*, 2001, **265**, 313 -322; (*b*) S. K. Pal, A. Krishnan, P. K. Das and A. G. Samuelson *J. Organomet. Chem.*, 2000, **604**, 248-259.

40   A. Otomo, G.L. Stegeman, M.C. Flipse, N.B. J. Diemeer, W.H.G. Horsthuis and G.R. Mohlmann, *J. Opt. Soc. Am. B*, 1998, **15**, 759.

41   (*a*) J. Kulhnek, F. Bureš, W. Kuznik, I. V. Kityk, T. Mikysek and A. Ruzicka, *Chem. Asian J.*, 2013, **8**, 465-475; (*b*) J. Kulhnek, F. Bureš, J. Opršal, W. Kuznik, T. Mikysek and A. Ruzicka, *Asian J. Org. Chem.*, 2013, **2**, 422-431.

42   I. Ledoux and J. Zyss, *Pure Appl. Opt.*, 1996, **5**, 603-612.

43   Z. Lin, Z. Wang, C. Chen and M.-H. Lee, *J. Chem. Phys.*, 2003, **118**, 2349-2356.

44   (*a*) S. K. Kurtz and T. T. Perry, *J. Appl. Phys.*, 1968,**39**,3798-3813; (*b*) J. P. Dougherty and S. K. Kurtz, *J. Appl. Cryst.*, 1976, **9**, 145-158.

45   O. Hammerich, in *Organic Electrochemistry*, 2nd Edn, Eds. M. Baizer, and H. Lund, Marcel Dekker, New York, 1983, Ch 16.

46   P. Zanello, in *Ferrocenes*, Eds. A. Togni and T. Hayashi, VCH, New York, 1995, Ch 7, pp. 317-430.

47   S. M. Batterjee, M. I. Marzouk, M. E. Aazab and M. A. El-Hashash, *Appl. Organometal. Chem.*, 2003, **17**, 291-297.

48   (*a*) G. Ahumada, T. Roisnel, S. Sinbandhit, C. Manzur, D. Carrillo and J.-R. Hamon, *J. Organomet. Chem.*, 2013, **737**, 1-6; (*b*) G. Ahumada, J. P. Soto, D. Carrillo, C. Manzur, T. Roisnel and J.-R. Hamon, *J. Organomet. Chem.*, 2014, **770**, 14-20.

49   (*a*) K. Das, A. Datta, S. Roy, J. K. Clegg, E. Garribba, C. Sinha and H. Kara, *Polyhedron*, 2014, **78**, 62-71; (*b*) N. Novoa, J. P. Soto, R. Henríquez, C. Manzur, D. Carrillo and J.-R. Hamon, *J. Inorg. Organomet. Polym. Mater.*, 2013, **23**, 1247-1254; (*c*) P. Pattanayak, J. Lal Pratihar, D. Patra, C.-H. Lin, S. Paul and K. Chakraborty, *Polyhedron*, 2013, **51**, 275-282; (*d*) O. Rotthaus, O. Jarjayes, C. Philouze, C. Pérez Del Valle and F. Thomas, *Dalton Trans.*, 2009, 1792-1800.

50   D. de Bellefeuille, M. S. Askari, B. Lassalle-Kaiser, Y. Journaux, A. Aukauloo, M. Orio, F. Thomas and X. Ottenwaelder, *Inorg. Chem.*, 2012, **51**, 12796-12804.

51   (*a*) K. Asami, A. Takashina, M. Kobayashi, S. Iwatsuki, T. Yajima, A. Kochem, M. van Gastel, F. Tani, T. Kohzuma, F. Thomas and Y. Shimazaki, *Dalton Trans.*, 2014,**43**, 2283-2293; (*b*) V. T. Kasumov, F. Köksal and A. Sezer, *Polyhedron*, 2005, **24**, 1203-1211; (*c*) E. Lamour, S. Routier, J.-L. Bernier, J.-P. Catteau, C. Bailly and H. Vezin, *J. Am. Chem. Soc.*, 1999, **121**, 1862-1869.

52   D.D. Perrin, W. L. F. Amarego and D. R. Perrin, *Purification of Laboratory Chemicals*, 2nd edn, Pergamon, New York, 1980.

53   V. V. Popic, S. M.; Korneev, V. A. Nikolaev, and I. K. Korobitsyna, *Synthesis*, 1991, 195-198.

54   A. Altomare, M. C. Burla, M. Camalli, G. Cascarano, C. Giacovazzo, A. Guagliardi, A. G. G. Moliterni, G. Polidori and R. Spagna, *J. Appl. Crystallogr.*, 1999, **32**, 115-119.

55   G. M. Sheldrick, *Acta Crystallogr., Sect. A: Fundam. Crystallogr.*, 2008, **64**, 112-122.

56   L. J. Farrugia, *J. Appl. Crystallogr.*, 2012, **45**, 849-854.

57   P. v. d. Sluis and A. L. Spek, *Acta Crystallogr., Sect. A: Fundam. Crystallogr.*, 1990, **46**, 194-201.

58   A. L. Spek, *J. Appl. Crystallogr.*, 2003, **36**, 7-13.

59   O. V. Dolomanov, L. J. Bourhis, R. J. Gildea, J. A. K. Howard and H. Puschmann, *J. Appl. Crystallogr.*, 2009, **42**, 339-341.

60   R. W. Terhune, P. D. Maker and C. M. Savage, *Phys. Rev.*, 1965, **14**, 681.

61   H. Le Bozec, T. Le Bouder, O. Maury, A. Bondon, I. Ledoux, S. Deveau and J. Zyss, *Adv. Mater.*, 2001, **13**, 1677-1681.

62   E. J. Baerends, D. E. Ellis and P. Ros, *Chem. Phys.*, 1973, **2**, 41-51.

63   (*a*) C. F. Guerra, J. G. Snijders, G. te Velde and E. J. Baerends, *Theor. Chem. Acc.*, 1998, **99,** 391-403; (*b*) G. te Velde, F. M. B ickelhaupt, E. J. Baerends, C. Fonseca Guerra, S. J. A. van Gisbergen, J. G. Snijder and T. Ziegler, *J. Comput. Chem.*, 2001, **22**, 931-967; (*c*) ADF2012, SCM, *Theoretical Chemistry*, Vrije Universiteit, Amsterdam, The Netherlands, http://www.scm.com.

64   J. P. Perdew, J. A. Chevary, S. H. Vosko, K. A. Jackson, M. R. Pederson, D. J. Sing and C. Fiolhais, *Phys. Rev. B*, 1992, **46**, 6671-6687.

65   E. Van Lenthe and E. J. Baerends, *J. Comput. Chem.*, 2003, **24**, 1142-1156.

66   (*a*) A. Klamt and G. Schüürmann, *J. Chem. Soc., Perkin Trans. 2*, 1993, 799-805; (*b*) A. Klamt, *J. Phys. Chem.*, 1995, **99**, 2224-2235; (*c*) A. Klamt and V. Jonas, *J. Chem. Phys.*, 1996, **105**, 9972-9981.

67   S. J. A. van Gisbergen, J. G. Snijders and E. J. Baerends, *Comp. Phys. Commun.*, 1999, **118**, 119-138.

68   P. J. Stephens, F. J. Devlin, C. F. Chabalowski and M. J. Frisch, *J. Phys. Chem.*, 1994, **98**, 11623-11627.

69   S. I. Gorelsky, *SWizard program*, revision 4.5, http://www.sg-chem.net/

70   G. Schaftenaar and J. H. Noordik, *J. Comput. Mol.*, 2000, **14**, 123-134.

# Table of contents entry

**Four-Coordinate Nickel(II) and Copper(II) Complexes Based ONO Tridentate Schiff Base Ligands: Synthesis, Molecular Structure, Electrochemical, Linear and Nonlinear Properties, and Computational Study**

**Nestor Novoa, Thierry Roisnel, Paul Hamon, Samia Kahlal,**

**Carolina Manzur, Hoang Minh Ngo, Isabelle Ledoux-Rak,**

**Jean-Yves Saillard, David Carrillo and Jean-René Hamon**

The spectroscopic, structural, and electrochemical properties of NLO active ternary nickel(II)- and copper(II)- unsymmetrical Schiff base complexes were explored in concert with DFT and TD-DFT calculations.